The Rotation Rates of Massive Stars: The Role of Binary Interaction through Tides, Mass Transfer, and Mergers

de Mink, S.E.; Langer, N.; Izzard, R.G.; Sana, H.; de Koter, A.

DOI
10.1088/0004-637X/764/2/166

Publication date
2013

Document Version
Final published version

Published in
Astrophysical Journal

The Astrophysical Journal, 764:166 (17pp), 2013 February 20 doi:10.1088/0004-637X/764/2/166

THE ROTATION RATES OF MASSIVE STARS: THE ROLE OF BINARY INTERACTION THROUGH TIDES, MASS TRANSFER, AND MERGERS

S. E. de Mink[1,2,7], N. Langer[3], R. G. Izzard[3], H. Sana[4], and A. de Koter[4,5,6]
[1] Space Telescope Science Institute, Baltimore, MD, USA
[2] Department of Physics and Astronomy, Johns Hopkins University, Baltimore, MD, USA
[3] Argelander-Institut für Astronomie der Universität Bonn, D-53121 Bonn, Germany
[4] Astronomical Institute Anton Pannekoek, University of Amsterdam, 1098 XH Amsterdam, The Netherlands
[5] Astronomical Institute, Utrecht University, 3508 TA Utrecht, The Netherlands
[6] Institute of Astronomy, KU Leuven, B-3001 Leuven, Belgium
Received 2012 September 9; accepted 2012 December 19; published 2013 February 4

ABSTRACT

Rotation is thought to be a major factor in the evolution of massive stars—especially at low metallicity—with consequences for their chemical yields, ionizing flux, and final fate. Deriving the birth spin distribution is of high priority given its importance as a constraint on theories of massive star formation and as input for models of stellar populations in the local universe and at high redshift. Recently, it has become clear that the majority of massive stars interact with a binary companion before they die. We investigate how this affects the distribution of rotation rates, through stellar winds, expansion, tides, mass transfer, and mergers. For this purpose, we simulate a massive binary-star population typical for our Galaxy assuming continuous star formation. We find that, because of binary interaction, 20^{+5}_{-10}% of all massive main-sequence stars have projected rotational velocities in excess of 200 km s^{-1}. We evaluate the effect of uncertain input distributions and physical processes and conclude that the main uncertainties are the mass transfer efficiency and the possible effect of magnetic braking, especially if magnetic fields are generated or amplified during mass accretion and stellar mergers. The fraction of rapid rotators we derive is similar to that observed. If indeed mass transfer and mergers are the main cause for rapid rotation in massive stars, little room remains for rapidly rotating stars that are born single. This implies that spin-down during star formation is even more efficient than previously thought. In addition, this raises questions about the interpretation of the surface abundances of rapidly rotating stars as evidence for rotational mixing. Furthermore, our results allow for the possibility that all early-type Be stars result from binary interactions and suggest that evidence for rotation in explosions, such as long gamma-ray bursts, points to a binary origin.

Key words: binaries: close – binaries: spectroscopic – Galaxy: stellar content – stars: early-type – stars: massive – stars: rotation

Online-only material: color figures

1. INTRODUCTION

The origins of the distribution of initial stellar masses and initial stellar rotation rates are not yet fully understood (e.g., Krumholz 2011; Rosen et al. 2012). For the latter, it is a key issue that stars inherit spin from their parental molecular clouds, whose specific angular momentum is orders of magnitude larger than what can be placed in a rotating star (e.g., Bodenheimer 1995). Based on the observations of low-mass pre-main-sequence and massive main-sequence stars, it appears that most stars reach the zero-age main sequence rotating significantly below their maximum possible rotation speed (e.g., Hartmann & Stauffer 1989; Huang et al. 2010). How angular momentum is expelled during the star formation process constitutes a classic problem (Mestel 1965; McKee & Ostriker 2007; Krumholz et al. 2009; Larson 2010). Observed rotation rates of stars on the zero-age main sequence provide important constraints for the theory of star formation. Unfortunately, massive stars become visible only once core hydrogen burning is already well underway (Yorke 1986) such that their initial rotational velocity distribution is not observationally accessible.

The embedding of massive stars in the early phases of their lives is indeed unfortunate as the initial rotation rate is thought to be a fundamental parameter determining their evolutionary fate, comparable to their initial mass and metallicity. Evolutionary models predict that rotation has major consequences for the core hydrogen-burning phase (Maeder & Meynet 2000b; Heger & Langer 2000; Hirschi et al. 2004; Yoon & Langer 2005; Brott et al. 2011b; Potter et al. 2012b; Ekström et al. 2012). Furthermore, there is growing evidence that in a fraction of massive stars, the final collapse and explosion is governed by rapid rotation, giving rise to hyper-energetic supernovae and long-duration gamma-ray bursts (Yoon et al. 2006; Woosley & Heger 2006; Georgy et al. 2009).

Several processes may affect the stellar rotation rates of massive main-sequence stars after they are born, causing deviations from the initial values. First, magnetic braking may cause them to spin down. In low-mass main-sequence stars magnetic breaking is ubiquitous, due to a dynamo process operating in their convective envelopes (Skumanich 1972; Soderblom et al. 1993). The fraction of more massive stars that show evidence for a magnetic field appears, however, to be smaller than about 15% (Donati & Landstreet 2009; Wade et al. 2012b).

Second, during core hydrogen-burning massive stars expand by about a factor of three. It appears, however, that a corresponding spin-down of the surface layers is prevented by an analogous contraction of the stellar core and by efficient transport of angular momentum from the core to the envelope (Ekström et al. 2008b; Brott et al. 2011a), independent of the detailed treatment of the internal angular momentum transport processes.

[7] Hubble Fellow.

The effects of main-sequence expansion on the surface rotation rates thus seem modest as well.

Third, even non-magnetic massive stars lose angular momentum due to their winds (Langer 1998). The winds of massive main-sequence stars, which are fairly well understood (Kudritzki & Puls 2000; Mokiem et al. 2007), are stronger at higher mass and metallicity (Vink et al. 2001) and for more rapid rotation (Friend & Abbott 1986). While for the majority of massive stars this wind-induced angular momentum loss can be neglected—for example, stars of Large Magellanic Cloud (LMC) composition below 14 $M_\odot$ lose less than 10% of their angular momentum this way (Langer 2012)—it can be important for O-stars and rapid rotators.

Finally—likely most important for the population of massive stars as a whole—are changes in the stellar spin due to close binary interaction. In recent decades, it has become evident that the majority of massive stars are formed in close binary systems (Mason et al. 1998, 2009; Sana & Evans 2011; Sana et al. 2012a). In these systems, the spin rate of both components can be drastically affected, by tides (e.g., Zahn 1975; Hut 1981; de Mink et al. 2009a), mass transfer (e.g., Packet 1981; Pols et al. 1991; Petrovic et al. 2005; Dervişoğlu et al. 2010), or when the two stars merge (e.g., Podsiadlowski et al. 1992; Tylenda et al. 2011). Sana et al. (2012b) showed that about two-thirds of all massive main-sequence O-stars are expected to strongly interact with a companion. In the majority of cases, after such interaction, either the binary is not expected to be recognized as such due to a large luminosity ratio and a large period, or there is no longer any binary due to merging or the breakup of the binary as a consequence of the supernova explosion of one star (de Mink et al. 2011; S. E. de Mink et al. 2013, in preparation). Consequently, any massive star population that is not extremely young contains a considerable number of apparently single stars whose spins are strongly altered by previous binary evolution.

In this paper we focus on the effects of binarity on the evolution of the rotation rates of a population of massive main-sequence stars. We do so by constructing binary population synthesis models that account for the latter three effects: the changing moment of inertia, wind losses, and—most importantly—binary interaction. It is our aim, after presenting our method and assessing the uncertainties, to compare our results with observed distributions of rotational velocities of massive main-sequence stars (e.g., Mokiem et al. 2006; Daflon et al. 2007; Wolff et al. 2008; Hunter et al. 2008b; Penny & Gies 2009; Huang et al. 2010; Dufton et al. 2013; O. Ramírez-Agudelo et al. 2013, in preparation). This will provide the first quantitative assessment of the difference between the initial rotational velocity distribution and the observed, present-day distributions.

2. CODE

We employ a rapid binary evolutionary code *binary_c* (Izzard et al. 2004, 2006, 2009) that makes use of fitting formulae (Hurley et al. 2000) to stellar models (Pols et al. 1998) to describe the structure of single stars as they evolve as a function of their mass, age, and metallicity. To study the effects of binary interaction by tides and winds and through mass transfer and mergers we use the evolutionary algorithms originally developed by Tout et al. (1997) and Hurley et al. (2002). These algorithms approximate the properties and evolution of a star after mass loss or mass accretion by switching to the prescriptions of a star with the appropriate mass, core mass, and relative age. These approximations enable us to follow the evolution of a particular binary system up to the remnant stage in less than a CPU second, which is needed to compute extensive grids of models that span the multi-dimensional parameter space characteristic for binary systems. In addition it allows us to explore the effects of uncertain parameters (cf. Izzard et al. 2009). For the purpose of this study we updated and extended various aspects of this code, which are described in the Appendix. A brief overview is given in the remainder of this section.

Throughout this paper, we present results in terms of the *"rotational velocity"* with which we refer to the tangential velocity due to rotation at the equator of the star, $v_{\rm rot}$. We account for the flattening of a rotating star assuming Roche geometry. In this approximation, the ratio of the radius at the equator and the polar radius becomes as large as $R_{\rm eq}/R_{\rm p} = 3/2$ when the star approaches the Keplerian limit, which is given by

$$\Omega_{\rm K} = \sqrt{GM/R_{\rm eq,K}^3}, \quad (1)$$

where G refers to the gravitational constant, M is the stellar mass, and $R_{\rm eq,K}$ is the equatorial radius of the star that rotates at the Keplerian limit. Equivalently, the Keplerian rotational velocity is given by

$$v_{\rm K} = \Omega_{\rm K} R_{\rm eq,K}. \quad (2)$$

To model deformation by rotation we use the fact that the polar radius is hardly affected by rotation. Even when the star rotates at the Keplerian limit the polar radius deviates by less than 2% from its non-rotating value for stars with masses between 3 and 20 $M_\odot$, and it deviates by less than 5% for stars with masses between 1 and 60 $M_\odot$ (Ekström et al. 2008b). This property allows us to use the stellar radii R_* in our code, which are based on non-rotating stellar models, as a good approximation for the polar radii of rotating stars, $R_{\rm p}(\omega) \approx R_{\rm p}(0) = R_*$, where we use the shorthand notation $\omega \equiv \Omega/\Omega_{\rm K}$. The equatorial radii can then be obtained by computing the shape of the Roche lobe as a function of the rotation rate, as is further explained in the Appendix.

To account for gravity darkening in stars rotating near their Keplerian limit, we assume that the maximum rotational velocity that can be observed is limited to a fraction $f_{\rm dark}$ of the Keplerian rotation rate. Based on Townsend et al. (2004) we adopt $f_{\rm dark} = 0.7$. Although this treatment is very simple, it reproduces the detailed simulations of Townsend et al. (2004) accurately enough for our purpose. Varying this parameter affects the extent of the high velocity tail in our distribution of rotation rates, but it does not have a significant effect on our main predictions.

Processes affecting all stars. We account for mass loss via stellar winds using prescriptions by Nieuwenhuijzen & de Jager (1990) and Vink et al. (2001) as described in Brott et al. (2011a). We treat the enhancement of stellar winds due to rotation as in Maeder & Meynet (2000a). As justified by Georgy et al. (2011), we assume mass loss through stellar winds to be spherical when computing the associated angular momentum loss. Details can be found in the Appendix. Our models do not account for effects of magnetic fields on angular momentum loss by stellar winds (e.g., Ud-Doula et al. 2009). We discuss the possible effects in Section 5.

As the star evolves along the main sequence, the outer layers expand while the core contracts. We account for changes in the moment of inertia using fitting formulae based on models by Pols et al. (1998); see the Appendix. The internal rotational profile is approximated assuming rigid rotation, which is a reasonable approximation for main-sequence stars (e.g., Brott et al. 2011a).

Processes affecting stars in close binaries. We include the effect of tides on the stellar spins and the stellar orbit (Zahn 1977; Hurley et al. 2002) and the transfer of angular momentum during mass transfer via an accretion disk or direct impact of the accretion stream onto the surface (Ulrich & Burger 1976; Packet 1981) as detailed in the Appendix. We assume that the initial stellar spins are aligned with the orbit. One of the main uncertainties in the treatment of binary interaction is the efficiency of mass transfer (e.g., de Mink et al. 2007). In particular, it is unclear how much stars can accrete after reaching the Keplerian limit. In our standard simulations we follow Paczynski (1991) and Popham & Narayan (1991) who argue that the accretion disk regulates the mass and angular momentum flux through viscous coupling allowing the star to continue to accrete. We do however limit the accretion rate by the thermal rate of the accreting star as described in the Appendix and in Hurley et al. (2002). In Section 5.2.2 we discuss the effect of this assumption. To account for systems that come in contact during the mass transfer phase we consider a critical mass ratio, $q_{\rm crit}$, as motivated in the Appendix. We assume that the stars come in contact when $M_{\rm acc}/M_{\rm don} < q_{\rm crit}$, where $M_{\rm don}$ is the mass of the Roche lobe-filling star and $M_{\rm acc}$ is the mass of the companion. In our standard simulations we adopt $q_{\rm crit,MS} = 0.65$ if the donor star is a main-sequence star, $q_{\rm crit,HG} = 0.4$ when the donor fills its Roche lobe when crossing the Hertzsprung gap. For a more evolved donor, we follow Hurley et al. (2002). The effects of these assumptions are discussed in Section 5.2.1. We assume that a merger product efficiently loses the excess angular momentum, such that it rotates at near Keplerian rotation when it has settled to its thermal equilibrium structure (Sills et al. 2005; Glebbeek et al. 2009). To account for mixing of fresh hydrogen into the central regions for accreting stars and mergers we follow Hurley et al. (2002). We assume that the convective core size adapts to the new mass and we describe this process using improved prescriptions for the effective mass of the convective core (Glebbeek & Pols 2008); see the Appendix. To be able to investigate the effect of the uncertainties related to stellar mergers we implement a parameterized prescription that allows us to explore extreme assumptions. In our standard simulations we assume that a fraction $\mu_{\rm loss} = 0.1$ of the total system mass is lost during the merger and that a small fraction $\mu_{\rm mix} = 0.1$ of the envelope is mixed into the convective core; see the Appendix. The effect of these assumptions is discussed in Section 5.

2.1. Simulating a Stellar Population

To investigate the effect of binary interaction on the distribution of rotation rates of early-type stars, we simulate a stellar population including binaries under the assumption of continuous star formation.

We approximate the distribution of the initial masses of single stars and the primary stars of binary systems as

$$f_{M_1}(M_1) dM_1 \propto M_1^{-\alpha} dM_1, \quad (3)$$

where M_1 denotes the mass of the primary star and $\alpha = 2.35 \pm 0.7$ (Salpeter 1955; Kroupa 2001). Even though one can argue whether an initial mass function that was derived for single stars can be applied to binary systems we note that the effect of this assumption on our results is small; see Section 5.

For the initial distribution of mass ratios, orbital periods, and the corresponding binary fraction we use the distributions in Sana et al. (2012b), which are based on extensive monitoring campaigns of O-stars in nearby young clusters (De Becker et al. 2006; Hillwig et al. 2006; Sana et al. 2008, 2009, 2011; Rauw et al. 2009). After correcting for biases, the authors find a binary fraction of 69% ± 9% for systems with mass ratios between 0.1 and 1 and orbital periods between $10^{0.15}$ and $10^{3.5}$ days. The distribution of orbital periods is described by

$$f_p(P) d\log P \propto (\log P)^{\pi} \, d\log P, \quad (4)$$

where $\pi = -0.55 \pm +0.2$. The distribution of mass ratios is described by

$$f_q(q) \, dq \propto q^{\kappa} \, dq, \quad (5)$$

where $q = M_2/M_1$, M_2 denotes the mass of the secondary star and $\kappa = -0.1 \pm 0.6$. Because these distributions are derived for a very young population, we assume that they well approximate the initial distribution functions of binary parameters. In our standard simulations we adopt $\alpha = 2.35$, $\pi = -0.5$, and $\kappa = 0$. The effects of varying these parameters are discussed in Section 5; see also Table 1.

Table 1
Impact of the Assumed Initial Binary Fraction and the Initial Distribution of Binary Parameters (as Defined in Section 2.1) on the Fraction F_r of Stars with $v \sin i > 200\,{\rm km\,s^{-1}}$

Initial Distribution	Variation	F_r (%)
Standard[a]		18.8
Orbital period	$0 > \pi > -1$	13.1–24.7
Mass ratio	$-1 < \kappa < 1$	14.8–21.3
Primary mass	$1.65 < \alpha < 3.05$	17.0–21.3
Binary fraction	$0.5 < f_{\rm bin} < 1.0$	14.6–23.9

Notes. For discussion, see Section 5.1.
[a] $\pi = -0.5$, $\kappa = 0.0$, $\alpha = 2.35$, and $f_{\rm bin} = 0.7$.

We do not include the effect of binaries with companions outside the range of orbital periods and mass ratios covered by Sana et al. (2012b) because the fraction of such systems is poorly constrained. As a result we may underestimate the effect of binaries. Systems with mass ratios more extreme than 0.1 may produce rapid rotators of early type if they interact during the main sequence of the primary and merge.

To reduce the dimensions of the parameter space, we assume circular orbits. Hurley et al. (2002) show that tides circularize the binary orbit just before the onset of mass transfer, implying that the effect of the initial eccentricity on the further evolution is small. By not considering the effect of very wide systems with high eccentricities we may underestimate the fraction of stars that interact.

The initial rotation rate of stars in a binary system does significantly affect the evolution of the binary system, except in extreme and rare cases (e.g., de Mink et al. 2009a). The reason is that the stellar spins at birth typically contribute at most a few percent to the total angular momentum budget of the system.

Since the rotational velocity distribution of massive stars at the zero-age main sequence is poorly constrained (see Section 1), we choose a very simple one that allows us to clearly demonstrate the effects of binary interaction. We adopt a uniform distribution for $v_{\rm rot}$ in the range 0–200 km s^{-1}, effectively assuming that stars are born with low to moderate rotation rates. While the upper limit of 200 km s^{-1} is not physically motivated, it will allow us to unambiguously identify the binary contribution to the formation of rapid rotators. Since the initial stellar spins are negligible compared to the

amount of angular momentum exchanged during mass transfer or merger, they do not affect the rotation rates of stars after these interactions. Although in future work adapting the initial spin distribution to reproduce the properties of suitable observed samples may be considered, this is beyond our present scope. To compute the distribution of projected rotation rates $v \sin i$, where i is the inclination angle of the binary system, we assume that the orientation of the binary orbits is random in space.

Unless an observational campaign is designed to detect binaries, many companion stars will remain undetected. We assume that only the rotation rate of the brightest star is measured in this case. Therefore, when constructing the simulated distribution of rotation rates, we only include the most luminous main-sequence star of each binary system.

For our standard simulation we adopt a metallicity of $Z = 0.008$, which is appropriate for the LMC. This metallicity is also considered representative for star-forming regions at a redshift 1–2, at the peak of star formation in the universe. The effect of metallicity is discussed in Section 4.1.

We derive the distribution of rotation rates for systems that are brighter than 10^4 and $10^5\,L_\odot$, respectively. To put this in perspective, in our models $10^4\,L_\odot$ corresponds to the luminosity of a 8.5–12 $M_\odot$ main-sequence star, depending on whether we take the model at zero-age or at the end of the main sequence. Similarly, a luminosity cutoff of $10^5\,L_\odot$ corresponds to stars with masses in excess of 20–28 $M_\odot$. Effectively, the first group is dominated by early B-type stars and the second group by O-type stars. We refrain at this stage from applying other cutoffs such as criteria based on temperature, color, or spectral type, since our predictions for the temperatures are less reliable than those for the luminosities.

3. THE EVOLUTION OF THE ROTATIONAL VELOCITY FOR INDIVIDUAL SYSTEMS

As a star evolves, its rotational velocity is affected by various processes, for example, as a result of angular momentum loss through stellar winds. While a single star can only lose angular momentum as a result of mass loss, a star in a binary system may either lose or gain angular momentum as it interacts with its companion. Even when angular momentum is conserved, the rotational velocity of a star can alter as a result of changes in the stellar interior. These effects are discussed in Section 3.1. The effect of binary interaction is discussed in Sections 3.2 and 3.3.

3.1. Effect of Changes in the Stellar Structure

Stars expand over the course of their main-sequence evolution. Although one might expect intuitively that the rotational velocity decreases as the star expands, in practice this is not the case. During the main sequence, contraction and consequent spin up of the core counteract the effect of the moderate expansion of the envelope. In this context, it is instructive to investigate how the moment of inertia, $I \sim kR^2$, changes as the star expands. Here, k denotes the square of the effective gyration radius, which depends on the internal density profile. If we approximate $k \sim R^{-\xi}$, or equivalently

$$\xi \equiv -\frac{d \ln k}{d \ln R}, \tag{6}$$

we find that the exponent ξ varies only slightly during the main sequence with typical values of 1.5–2. In the case of rigid rotation, we can now express how the rotation rate Ω, the rotational velocity $v_{\rm rot}$, and the ratio of the rotation rate and the Keplerian rate $\omega/\omega_{\rm K}$ change as the star expands,

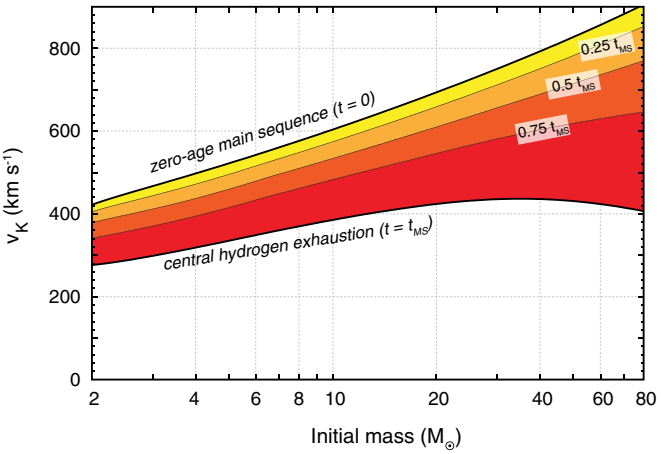

Figure 1. Evolution of the Keplerian rotational velocity for stars of different initial masses during their main-sequence evolution. Labels show the relative age as a fraction of the main-sequence lifetime $t_{\rm MS}$. This diagram is constructed using stellar radii from Pols et al. (1998) for a metallicity of $Z = 0.008$, using the prescription by Hurley et al. (2000). We note that the time-dependent radii for stars more massive than about 40 $M_\odot$ are very uncertain. In the most massive stars the decrease of the Keplerian velocity with time may well be more severe than shown here. See Section 3.1 for a discussion.

(A color version of this figure is available in the online journal.)

$$\frac{d \ln \Omega}{d \ln R} = \xi - 2, \tag{7}$$

$$\frac{d \ln\, v_{\rm rot}}{d \ln R} = \xi - 1, \tag{8}$$

$$\frac{d \ln \Omega/\Omega_{\rm K}}{d \ln R} = \xi - \frac{1}{2}. \tag{9}$$

In other words, given typical values of ξ, we find that the decreasing gyration radius compensates for the expansion of the star such that the rotation rate Ω decreases only slightly as the star evolves (Equation (7)), since $d \ln \Omega / d \ln R \approx -0.5{-}0$. The rotational velocity at the equator, $v_{\rm rot}$, increases slightly (Equation (8)).

Most interestingly, the last expression shows that stars naturally evolve toward the Keplerian limit (Equation (9)), if the amount of angular momentum loss is small and internal angular momentum transport between the core and envelope is efficient. An important implication of this is that when a star reaches the Keplerian rotation rate, it remains rotating near the Keplerian limit in the absence of an efficient angular momentum loss mechanism. We refer the reader to the excellent discussion by Ekström et al. (2008b), which describes this effect in detailed models of single stars that allow for differential rotation.

Figure 1 shows the Keplerian rotational velocity $v_{\rm K}$ as a function of the initial mass of a star at different stages during the main sequence. In zero-age main-sequence stars the Keplerian velocity increases monotonically with the initial stellar mass. The Keplerian velocity drops as stars evolve and expand. The largest change occurs during the final stages of main-sequence evolution. The change in radius of more massive stars during the main sequence is larger, resulting in a more significant drop in the Keplerian velocity. As a result, the Keplerian rotational velocity at the end of the main sequence is around 400 km s^{-1} with only a weak dependence on the stellar mass. Note that

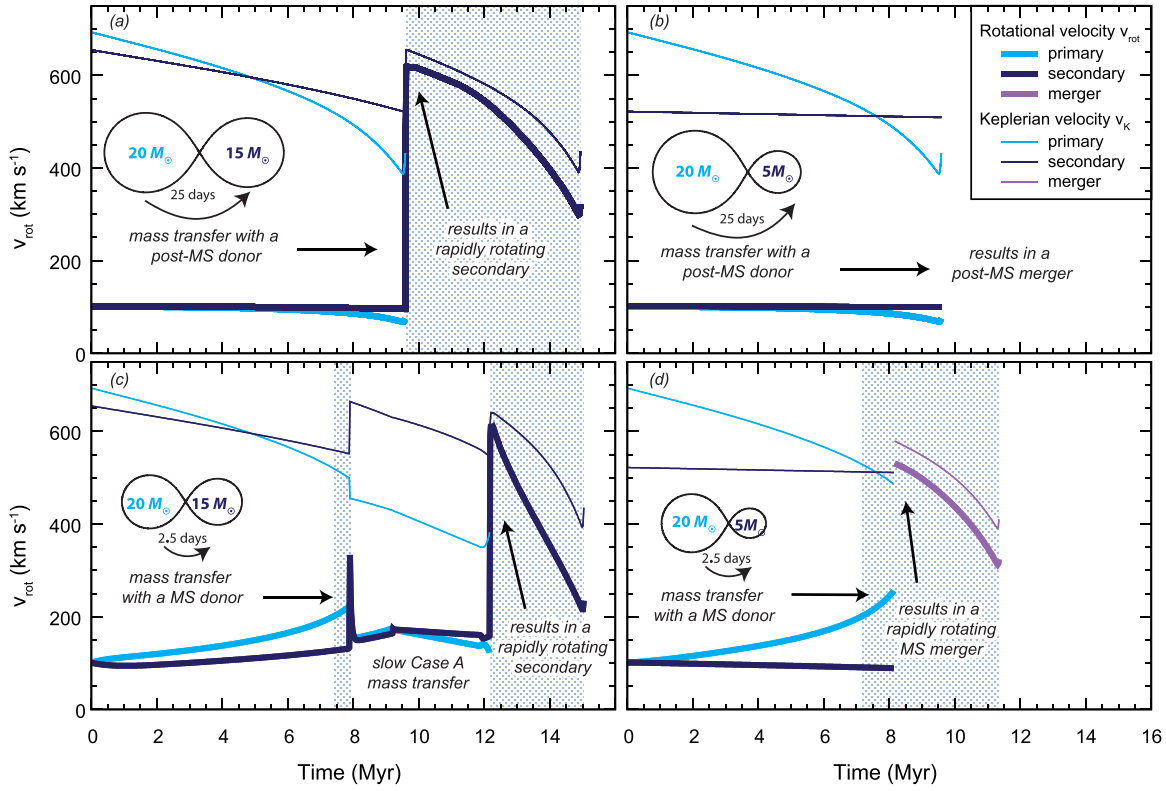

Figure 2. Four annotated examples of the effect of binary interaction on the stellar rotation rates of main-sequence stars for systems with different initial mass ratios (left vs. right panels) and different initial orbital periods (upper vs. lower panels) for $Z = 0.008$. Each panel shows the evolution of the equatorial rotational velocity $v_{\rm rot}$ of the primary and secondary star (thick lines) as well as the Keplerian rotational velocity $v_{\rm K}$ (thin lines) as long as the stars are on the main sequence. Shading highlights the phases during which one of the stars is rotating more rapidly than 200 km s^{-1}. See Section 3.2 for more information.

(A color version of this figure is available in the online journal.)

the projected rotational velocity for such a star accounting for gravity darkening is considerably smaller, by a factor of $f_{\rm dark}\langle \sin i \rangle \approx 0.55$.

We note that the amount by which the massive stars expand over the main sequence is not well constrained. The models on which this diagram is based (Pols et al. 1998) have been calibrated to the radii of eclipsing binaries of intermediate mass (Pols et al. 1997; Schröder et al. 1997). In these models the expansion of massive stars over the course of the main sequence is limited to a factor of 2–3. In contrast, the models by Brott et al. (2011a), which adopt a larger value for the overshooting parameter, predict expansion by a factor of 3–5 for stars in the mass range 5–30 $M_\odot$. While the predictions based on models with both codes show excellent agreement at zero age, the Keplerian velocities at the end of the main sequence are smaller by about a factor of 2 in the Brott et al. (2011a) models.

Furthermore we note that in the most luminous stars the effects of radiation pressure cannot be ignored and the Keplerian limit should be considered as an upper limit to the physical maximum.

3.2. Examples of the Spin Evolution of Binary Systems

In Figure 2 we depict four examples of the evolution of the rotational velocity for main-sequence stars in a binary system. In each example, we assumed an initial mass for the primary star of 20 $M_\odot$, a metallicity of $Z = 0.008$, and initial rotational velocities of 100 km s^{-1} for both stars. In the top row we show systems with initial orbital periods of $P = 25$ days. These systems are so wide that the primary star fills its Roche lobe only after it leaves the main sequence as it expands during its hydrogen shell burning phase. In the bottom row we assumed an initial orbital period of $P = 2.5$ days. In these tight systems the primary star fills its Roche lobe as a result of expansion on the main sequence.

The panels on the left show examples in which the initial mass of the secondary is comparable to that of the primary, $M_2/M_1 = 0.75$. In these examples, one or more phases of mass transfer eventually lead to spin-up of the companion star. In the panels on the right we adopted a more extreme initial mass ratio, $M_2/M_1 = 0.25$. In these systems the onset of mass transfer brings the stars into contact and they merge. Only in the short-period case are the two stars that merge both still main-sequence stars. After the merged star regains its thermal equilibrium, it is expected to continue to burn hydrogen in the center.

The phases during which one of the stars is rotating more rapidly than 200 km s^{-1} are highlighted in Figure 2 with gray shading. Note that during the major part of this phase, the rapidly rotating star is single or appears to be single. The clearest example is shown in panel (d) where the rapidly rotating star is the product of a merger between the two stars. In panels (a) and (b) the rapidly rotating star is the spun-up secondary. The primary star has lost its hydrogen envelope and is hard to detect, as a result of its reduced mass, its low luminosity, and the wide orbit. When the primary star finishes its nuclear burning and explodes, it is likely to disrupt the system, leaving the rapidly rotating secondary behind as a single star.

Besides the drastic effects of mass transfer and coalescence, Figure 2 illustrates the other processes that have a more subtle effect on the stellar rotation rates, which we describe below.

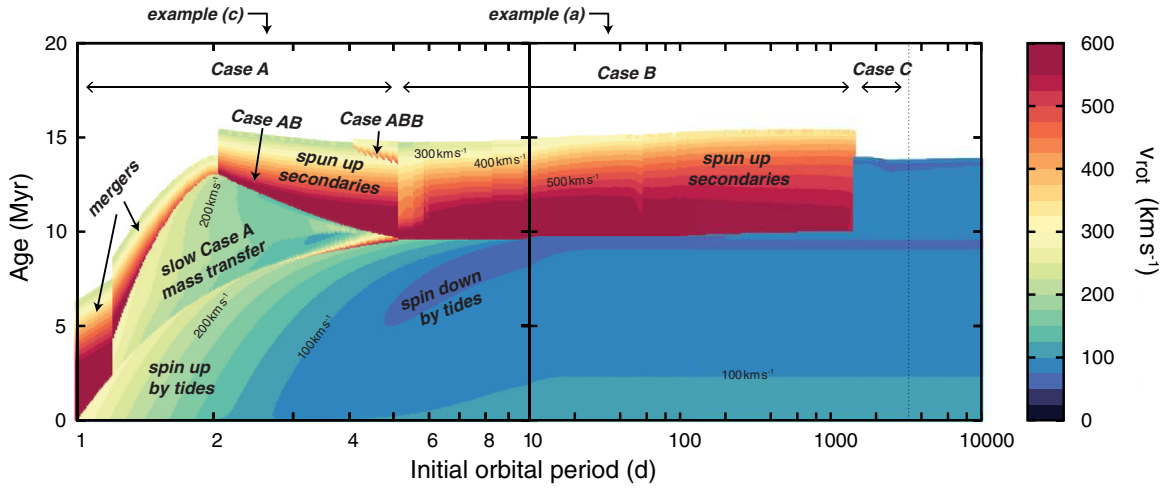

Figure 3. Rotational velocity (color shading) as a function of initial orbital period and time for the brightest main-sequence star in a binary system. We adopt initial masses of 20 and 15 $M_\odot$, initial rotational velocities of 100 km s^{-1}, and a metallicity of $Z = 0.008$. As the stars evolve along the main sequence their rotational velocity is altered by stellar winds, internal evolution, tides, and most notably mass accretion. The vertical dotted line indicates the maximum separation for which this system interacts by mass transfer. The examples shown in panels (a) and (c) of Figure 2 are part of this simulation.

(A color version of this figure is available in the online journal.)

Changes in the stellar structure. The effect of changes on the stellar structure as the star evolves can be observed, for example, in panel (a) of Figure 2. During the first 9.5 Myr of the evolution of this system both stars reside well within their Roche lobe and their evolution is similar to that of single stars. The rotational velocity of both stars remains roughly constant during this phase (cf. Section 3.1). When the primary star approaches the end of its main-sequence lifetime, its expansion accelerates. This leads to the decrease of the rotational velocity that is visible in panel (a) at an age of 8–9.5 Myr. The expansion is also responsible for the decrease of the Keplerian rotational velocity with time.

Stellar wind. The effect of angular momentum loss by stellar winds is small during the major part of the main sequence in these examples. The winds become stronger toward the end of the main sequence, which together with the expansion, contributes to the decrease in the rotational velocity of the primary discussed above. However, spin-down by winds does play a significant role for the massive, rapidly rotating stars that can be produced as a result of mass transfer. This effect can be seen most clearly in panel (c) for ages of 12–15 Myr. The secondary quickly spins down, reducing its rotational velocity by about a factor of 3.

Tides. Tidal interaction tends to synchronize the rotation of the stars with the orbit in systems where the separation between the stars is comparable to the stellar radii. The systems depicted in the upper and lower panels have initial separation on the order of 120 $R_\odot$ and 40 $R_\odot$, respectively; this is slightly less for the systems on the right due to the smaller mass ratios. Tides do not play a significant role during the main sequence of the stars in the upper panels, but they are responsible for the gradual increase in rotational velocity that can be seen in the lower panels for the primary star during the first 8 Myr. The orbital period remains nearly constant during this phase. The primary star is kept in corotation with the orbit as it expands, which implies that the rotational velocity gradually increases. In this example, the primary expands by just over a factor of two before it fills its Roche lobe, resulting in a rotational velocity in excess of 200 km s^{-1}.

In panel (c) of Figure 2, tides are also important for the secondary star, during the first mass transfer phase, which starts at about 8 Myr. The secondary star spins up as it accretes mass and angular momentum. However, the tides quickly spin the star down to synchronous rotation. This system experiences a mass transfer phase, which lasts almost 4 Myr, during which both stars remain in synchronous rotation while the orbit gradually widens. Around 12 Myr a second rapid phase of mass transfer sets in, i.e., Case AB, as the primary star leaves the main sequence and expands during hydrogen shell burning. As a result of the high-mass transfer rate and the fact that the orbit widens, tides are no longer effective in preventing the accreting star from spinning up.

3.3. Effect of the Initial Separation and Mass Ratio

To further illustrate the effect of the initial binary parameters, we depict in Figure 3 the evolution of the rotational velocity of the brightest main-sequence star in a binary system as a function of the initial orbital period. For this example we adopted an initial rotation rate of 100 km s^{-1}, a metallicity of $Z = 0.008$, and initial masses of 20 and 15 $M_\odot$. The color shading indicates the equatorial rotational velocity of the brightest main-sequence star in each system. Initially this is the primary star, but after mass transfer the secondary becomes the brightest.

Mass transfer with a main-sequence donor (Case A). In short-period systems the expansion of the primary star during its main-sequence evolution is sufficient to make it fill its Roche lobe. These systems experience a phase of slow mass transfer that can last for several Myr. Mass transfer typically occurs via direct impact onto the surface of the secondary. Tides keep both stars synchronized, which prevents the secondary from reaching very high rotation rates. This phase ends when the two stars come into contact and merge (for periods $P \lesssim 2$ days) or when the primary star leaves the main sequence (for periods $P \approx 2$–5 days), triggering a new mass transfer phase (Case AB). Both cases are expected to lead to the formation of a massive rapidly rotating star. In certain cases the rapidly rotating star experiences an additional spin-up phase, when the primary fills its Roche lobe again as it expands during He shell burning (Case ABB). This effect is visible in Figure 3 around 14 Myr for systems with orbital periods of 4–5 days.

The rapidly rotating stars resulting from such close binaries are typically more massive than the original primary. As a result of their high mass and large luminosity, their remaining lifetime is short compared to the rapid rotators resulting from wider systems and they experience more efficient spin down by their stellar winds, as can be seen in Figure 3.

The type of evolution described in this section is representative of systems with comparable initial masses for the primary and secondary star. In systems with more extreme mass ratios, the secondary star is predicted to swell up and fill its Roche lobe as well directly after the onset of mass transfer. If the two stars evolve into a contact situation it is expected that mass is lost via the outer Lagrangian point, effectively draining angular momentum from the system. This drives the stars into deeper contact. We assume that such systems will merge to form a rapidly rotating single star.

Mass transfer with a post-main-sequence donor (Case B). Systems wider than about five days interact when the primary star expands after core hydrogen exhaustion as it crosses the Hertzsprung–Russell diagram on its way to becoming a red supergiant. This happens during hydrogen shell burning (for periods $P \approx$ 5–100 days) or after the ignition of helium (for periods $P \approx$ 100–1000 days).[8] The period ranges quoted here are only rough indications; they depend on the mass of the donor star and on metallicity.

Mass accretion in these systems occurs typically via an accretion disk. The companion is quickly spun up, approaching the Keplerian velocity after accreting only a few percent of its own mass. According to Popham & Narayan (1991) mass accretion continues after the star has reached Keplerian rotation as viscous processes transport excess angular momentum outward. The outer edge of the disk is truncated by tides and feeds the excess angular momentum back to the orbit.

The mass transfer rate is higher for wider systems, in which the donor is more evolved. In our standard simulations, the mass accretion rate is limited by the thermal rate, $M_*/\tau_{\rm KH}$, of the accreting star, where $\tau_{\rm KH}$ is the Kelvin–Helmholtz timescale. This is independent of the separation. As a result we find the general trend that tighter systems evolve more conservatively, resulting in more massive secondaries in comparison with wider systems. The more massive secondaries have stronger stellar winds which cause them to spin down more quickly in comparison to less massive secondaries. This effect can be seen in the steepness of the color gradient in Figure 3. Compare, for example, the change of rotation rate with time for a rapid rotator resulting from a binary with an initial orbital period of about 5.5 days with the rapid rotators resulting from wider systems.

Surprisingly, the remaining main-sequence lifetime of the secondary is roughly independent of the amount of accreted mass or orbital period. This is a consequence of two counteracting effects. The higher stellar mass implies shorter evolutionary timescales, i.e., a reduction of the remaining lifetime. At the same time mass accretion results in mixing of fresh hydrogen into the central regions, extending the remaining lifetime.

Systems with extreme mass ratios are expected to enter a phase of common envelope evolution soon after the onset of mass transfer. The tighter systems result in a merger, but the product is a post-main-sequence star, either a blue or red supergiant. Although such mergers are very interesting, in this paper we focus on main-sequence stars, so we do not include these in further discussion. In wider systems where the binding energy of the envelope of the primary is smaller and the momentum and energy in the orbit are larger, the envelope can be ejected. This process is so fast that it is not expected to significantly affect the secondary star. So, we assume that its rotation rate is unaffected. The only exceptions are systems that are just wide enough to avoid a merger, but in which the ejection of the envelope results in significant shrinking of the orbit, such that tides lock the orbit of the secondary to the orbit of the naked core of the primary star. Such systems experience a second phase of mass transfer when the primary expands during helium shell burning. However, these systems are rare. They do not significantly contribute to the population of rapidly rotating stars resulting from binary evolution.

Mass transfer with supergiant donor (Case C). In the widest binaries, $P \approx$ 1500–3000 days in our simulations, the donor star develops a convective envelope before it fills its Roche lobe. When it loses mass we assume it reacts by expanding, resulting in very high mass transfer rates (see, however, Woods & Ivanova 2011). As the Roche lobe typically shrinks, this leads to a runaway situation resulting in a common envelope phase. In our simulations these systems eject the envelope, leaving the secondary star and its spin relatively unaffected.

A common envelope phase is expected for a very wide range of mass ratios. Only systems with initial mass ratios close to one can avoid this phase; see, for example, Claeys et al. (2011).

4. THE DISTRIBUTION OF PROJECTED ROTATIONAL VELOCITIES

We simulate the distribution of projected rotational velocities for a population of main-sequence stars consisting of single stars and stars in binary systems by assuming continuous star formation and a uniform distribution of low to intermediate rotational velocities $v_{\rm rot} < 200\,{\rm km\,s^{-1}}$ at birth, as described in Section 2. The central panels of Figure 4 show the resulting distributions, $f(v \sin i)$, using a bin size $\Delta v \sin i = 10\,{\rm km\,s^{-1}}$. The upper and lower panels show our results for brightness cutoffs of 10^4 and $10^5\,L_\odot$, respectively (Section 2). The corresponding cumulative distributions,

$$F(v \sin i) = \sum_{0}^{v \sin i} f(v \sin i)\,\Delta v \sin i, \qquad (10)$$

are shown in the panels on the left.

For a luminosity limit of $10^4\,L_\odot$, the resulting $v \sin i$ distribution is bimodal. The majority of the stars have low to intermediate rotational velocities, whereas nearly one-fifth has rotational velocities in excess of $200\,{\rm km\,s^{-1}}$, i.e., larger than the maximum of the assumed distribution at birth. The first group consists predominantly of single stars and members of binary systems that have not interacted through Roche lobe overflow. The rapid rotators consist almost exclusively of stars that are the product of Roche lobe overflow. The top right panel of Figure 4 shows that this group consists mainly of stars that gained mass and angular momentum by mass transfer. A smaller number are merger products of stars, i.e., stars resulting from the coalescence of two main-sequence stars in a contact binary.

For stars above $10^5\,L_\odot$, the shape of the distribution changes as can been seen in the two central panels. The distribution

[8] Note that part of this group is indicated as Case C in the classical classification scheme (Kippenhahn & Weigert 1967; Lauterborn 1970), which is based on models for lower mass stars at solar metallicity that reach giant dimensions before helium ignition. In our example, helium is ignited at smaller radii. Since this group behaves similar to Case B systems we discuss them in this section.

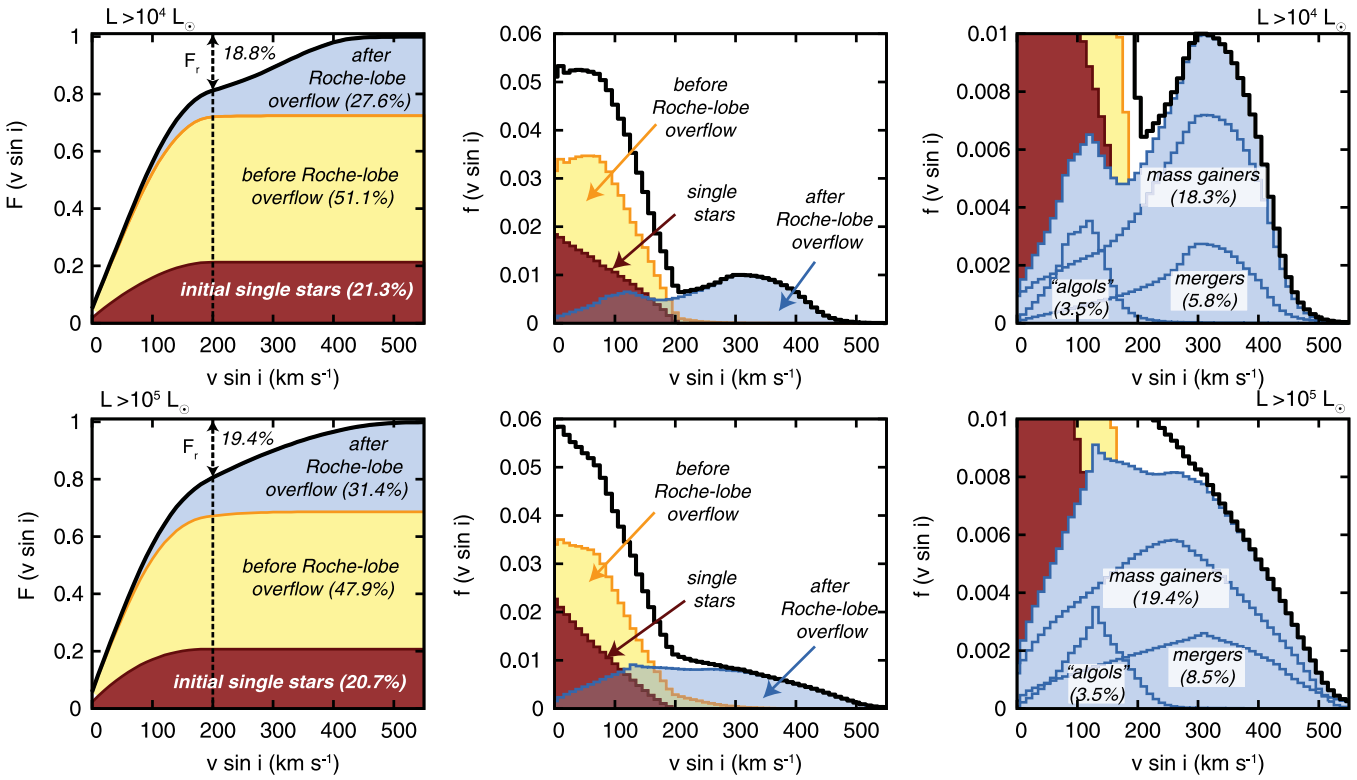

Figure 4. Projected rotation rate distribution for a population of main-sequence stars assuming continuous star formation. The top and bottom rows show results including only stars or systems brighter than 10^4 and 10^5 $L_\odot$. The left panels show the cumulative distribution function indicating the fraction of stars F_r with projected rotational velocities larger than 200 km s^{-1}. The center and right panels show the full distribution function and a zoom-in highlighting the contribution of the various binary products. See Section 4 for further explanation.

(A color version of this figure is available in the online journal.)

shown in the upper panel shows two separated components. Instead, the rapid rotators shown in the lower panel form a tail or plateau that merges with the main component at lower $v \sin i$. This difference is the result of angular momentum loss through stellar winds, which is stronger for the brighter stars. Even though the brightest stars are included in both distributions, the distribution in the upper panel is dominated by the less bright stars, since the initial mass function favors lower mass stars.

A further difference between the upper and lower plots in the central panel of Figure 4 is that the bright star distribution extends to higher rotational velocities. The reason is that many binary products rotate near their Keplerian limit, which is larger for the brighter, more massive stars (cf. Figure 1).

Not all binary products have large projected rotational velocities. Apart from rapid rotators observed at small inclinations, i.e., nearly pole-on, there is a small contribution from systems that are undergoing mass transfer, indicated with the shorthand "Algols" in Figure 4. This group consists almost entirely of short-period systems that are undergoing a slow, i.e., nuclear timescale, Case A mass transfer (cf. Section 3). The rotational velocity reflects the rotation rate of the accreting star, which has become the brightest star in the system. Even though this star is accreting mass and angular momentum, tides are efficient enough, during this slow phase of mass transfer, to prevent it from spinning rapidly. These systems are easily detected as binaries. As the donor star fills its Roche lobe these systems are likely to show eclipses or at least ellipsoidal variations. Examples of such systems are the 30 semi-detached systems in the sample of double-lined eclipsing binaries by Hilditch et al. (2005).

The distribution of the rotational velocities of single stars closely resembles the adopted uniform birth distribution. The apparent bias toward low rotational velocities is only partially due to spin-down by stellar winds and changes in the stellar structure. The main reason is the projection effect caused by the random distribution of spin axis of the stars.

The rotational velocities of stars in binary systems that have not yet interacted by Roche lobe overflow can be affected by tides. The effect of spin-up by tides can be seen in the yellow-shaded area as a tail of stars rotating between 200 and about 300 km s^{-1}, which is most pronounced in the lower central panel. Tides are also responsible for the flattening of the yellow curve for pre-Roche lobe overflow systems below 100 km s^{-1}, as they counteract the spin-down toward the end of the main sequence which is imposed by stellar winds and stellar expansion. Even though tides may also lead to spin-down, they do not produce very slow rotators, since slow synchronized rotation implies wide orbits and tides are no longer effective in wide binaries.

We have included mergers separately in Figure 4, to show how the distribution may change if mergers behave differently than we have assumed in our simulations (see Section 5.2 for further discussion).

4.1. Metallicity Dependence

The metallicity affects the distribution of rotational velocities via its effect on the stellar wind and on the stellar structure. In Figure 5 we show the normalized distribution of rotational velocities for main-sequence stars brighter than 10^5 $L_\odot$ for a range of metallicities. We assume here that the initial mass function,

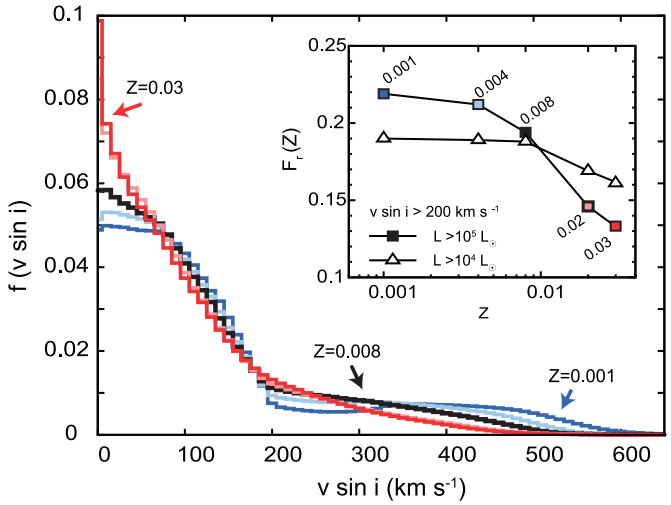

Figure 5. Distribution of projected rotational velocities $f(v \sin i)$ for different metallicities ranging from $Z = 0.001$ (blue line) to 0.03 (red line) for systems brighter than $L > 10^5\,L_\odot$ containing at least one main-sequence star. The inset gives the color code and summarizes the effect of metallicity by showing the fraction of stars F_r with projected rotational velocities larger than 200 km s^{-1}, i.e., see Section 4.1 for further information.

(A color version of this figure is available in the online journal.)

the binary fraction, and the binary distribution functions are not dependent on metallicity.

At the lowest metallicities shown, the distribution consists of two distinct components with broad peaks at $v \sin i \sim 100$ and 400 km s^{-1}. It resembles the distribution shown in the top panels of Figure 4 for $10^4\,L_\odot$, although the low-metallicity distribution extends to velocities as high as 600 km s^{-1}. At the highest metallicity the two components merge to one smooth distribution with a strong peak at $v \sin i \simeq 0$ km s^{-1}.

The inset in Figure 5 shows the fraction of stars with projected rotational velocities in excess of 200 km s^{-1}, F_r, as a function of metallicity, Z. This fraction is in the range 13%–22%, with larger values for smaller metallicities, and a stronger metallicity dependence for more massive stars. These trends are mainly the result of the dependence of the stellar winds on metallicity and brightness, and the corresponding wind-induced angular momentum loss.

Additionally, main-sequence stars tend to be more compact at lower metallicity, where hydrogen burning via the CNO cycle operates less efficiently. More compact stars have higher Keplerian rotational velocities for the same mass. This is reflected in the extent of the high velocity tail in Figure 5 which increases with decreasing metallicity. Furthermore, the smaller radii imply somewhat more compact binary systems, which raises the importance of tidal interactions at low metallicity.

5. EFFECTS OF UNCERTAINTIES IN THE ADOPTED ASSUMPTIONS

In this section we take advantage of the speed of our rapid binary evolutionary code and population synthesis routines, which enables us to evaluate the impact of our assumptions. This concerns the initial distribution functions (Section 5.1) and assumptions about the physics of binary evolution (Section 5.2). We quantify the effects by comparing the fraction of stars with projected rotational velocities in excess of 200 km s^{-1}, F_r, that results from the various assumptions. We use our standard simulation for $L > 10^4\,L_\odot$ as reference.

5.1. Initial Distribution Functions

The effect of uncertainties in the adopted initial distributions is relatively small, each affecting the fraction of rapid rotators only by a few percent in absolute terms; see Table 1. The *initial orbital period* distribution is the largest cause of uncertainty accounting for a variation of ±5.8%. When we compare a distribution that is flat in log P, i.e., Öpik's law ($\pi = 0$), to a distribution that strongly favors short-period systems ($\pi = -1$), we find that F_r increases from 13.1% to 24.7%. The latter distribution favors systems that interact while the primary star is still on the main sequence. In our simulations, these systems produce rapid rotators through mass transfer and mergers that are on average more massive, and thus brighter, than rapid rotators produced in wider binaries.

Uncertainties in the adopted *distribution of mass ratios* are responsible for a variation of just over ±3% when we vary the power-law exponent from $\kappa = -1$ to $\kappa = 1$, which generously allows for the uncertainties quoted by Sana et al. (2012b). A distribution skewed toward systems with comparable masses for the components ($\kappa = 1$) favors systems that produce rapid rotators through nearly conservative mass transfer. The spun-up mass gainers are typically brighter than the original primary, and they experience significant rejuvenation. Both effects result in a larger fraction of rapid rotators in the population. A distribution that favors systems with extreme mass ratios ($\kappa = -1$) results in a larger number of mergers. While mergers in short-period systems contribute to the fraction of rapid rotators, mergers resulting from wider systems do not, as we consider these to become post-main-sequence objects, explaining the reduction of the fraction of rapid rotators.

The rapid rotators in our simulation result from stars that gain mass, apart from the small contribution of tidally spun-up stars. On average a gain in mass implies a larger luminosity. Stars that were initially not bright enough to be included in our distribution can become sufficiently bright after accreting. Changing the relative number of lower mass systems, by adopting the *initial mass function*, increases the number of potential systems that can produce rapid rotators. However, the effect is small: varying the steepness of the initial mass function of the primary star by $\alpha = 2.35 \pm 0.7$ leads to a change of about ±2%.

The effect of varying the initial binary fraction can be obtained by rescaling the results. We account for the fact that the fraction of stars born as single stars in the population F_s is not equal to the fraction of single stars at birth. The fraction of rapid rotators F_r for any given initial binary fraction $f_{\rm bin}$ is given by

$$F_r(f_{\rm bin}) = F_r^* \frac{f_{\rm bin}}{f_{\rm bin}^*} \left(F_b^* \frac{f_{\rm bin}}{f_{\rm bin}^*} + F_s^* \frac{1 - f_{\rm bin}}{1 - f_{\rm bin}^*} \right)^{-1}, \qquad (11)$$

where the superscript * refers to the values obtained in our standard simulation (see Figure 4) and $F_b = 1 - F_s$. Considering a population in which only half or all stars are born as binaries with mass ratios and orbital periods as specified in Section 2.1 results in variations in F_r of about ±5%.

5.2. Uncertain Physics

In this section we address uncertain physical assumptions regarding the treatment of mass transfer, the formation of contact systems, and mergers.

5.2.1. Do Contact Systems Merge?

Mass accretion drives the companion star out of thermal equilibrium causing it to expand when the mass transfer timescale is

short compared to the thermal timescale of the companion (e.g., Neo et al. 1977). This can lead to the formation of a contact binary (Pols 1994; Wellstein et al. 2001). However, the parameter range for which contact occurs is uncertain as it depends, among other things, on the poorly constrained specific entropy of the accreted material (Shu & Lubow 1981).

When contact is established, it is not clear whether this always leads to a common envelope phase and a merger. If the secondary star overfills its Roche lobe by only a small amount, the star may detach again as the star restores thermal equilibrium (de Mink et al. 2007). However, the outcome depends on mass and angular momentum loss during this phase. If the stars come into deep contact, mass loss from the system through the outer Lagrangian point efficiently drains angular momentum from the system and drives the stars deeper into contact. Mass loss through stellar winds or bipolar outflows can, in principle, have the opposite effect.

In our standard simulation we account for the formation of contact due to rapid mass transfer by considering the mass ratio $q = M_2/M_1$ at the onset of Roche lobe overflow. If the mass ratio is smaller than a critical value we assume that contact is established and results in a merger. If the mass ratio is larger, we continue to compute the accretion of mass and angular momentum onto the secondary star, and assume that contact is avoided as long as the thermal equilibrium radius of the mass gainer is smaller than its Roche radius. Below, we discuss the impact on our results of varying the adopted critical mass ratio systems that interact during the main sequence $q_{\rm crit,MS}$ and systems in which the donor star is a post-main-sequence star crossing the Hertzsprung gap $q_{\rm crit,HG}$.

Contact involving two main-sequence stars. Systems that interact during the main sequence eventually produce a rapid rotator either through a merger or through spin-up during mass transfer regardless of their initial mass ratio. Therefore, the fraction of rapid rotators is not very sensitive to the adopted critical mass ratio for merging $q_{\rm crit,MS}$. In our standard simulation we adopted $q_{\rm crit,MS} = 0.65$. If we vary $q_{\rm crit,MS}$ in the range 0.8–0.25, the fraction of rapid rotators changes by only $\pm 0.5\%$. On the one hand, mergers are typically more massive and more luminous than the secondary star would have been had the system not merged. As a result, in our brightness-limited sample the rapidly rotating stars resulting from mergers originate from binary systems with a wide range of initial masses and mass ratios. On the other hand, we find that the remaining relative lifetime of mergers is typically much smaller than that of rapid rotators produced through mass transfer. Mergers contain the helium-rich core of the original primary and even though some fresh hydrogen is mixed into the central regions, their remaining lifetime is limited. In contrast, the core of the secondary is still hydrogen rich at the onset of mass transfer in comparison to the core of the primary. In the population, the longer remaining lifetime of the secondaries compensates for their lower brightness.

Contact involving the Hertzsprung gap donor. For post-main-sequence interaction the formation of contact introduces a larger uncertainty on the predicted number of rapid rotators. If a binary system mergers after the primary star has left the main sequence, the product is expected to become a post-main-sequence object, a blue or a red supergiant. Hence, we do not include such stars in our distribution of rotation rates. In our standard simulation we assume that such systems merge if the mass ratio at the onset of Roche lobe overflow is smaller than $q_{\rm crit,HG} = 0.4$. Detailed binary evolutionary models show that the parameter range for the formation of contact may be substantially larger (e.g., Wellstein et al. 2001). For the extreme assumption that all these systems merge we find an absolute change of -5.4% for the fraction of rapid rotators. To obtain this estimate, we mimic the results of Wellstein et al. (2001) by assuming that all systems with initial orbital periods larger than 30 days and mass ratios smaller than 0.65 merge. Even though this assumption affects a very large fraction of the initial parameter space, the effect is limited because it mostly affects systems that would produce relatively low mass rapid rotators. Taking the opposite extreme assumption that none of the Case B systems merge ($q_{\rm crit,HG} = 0.0$) does have a significant effect on the fraction of rapid rotators, for the same reasons.

5.2.2. Can Stars Continue to Accrete after they are Spun Up to Keplerian Rotation?

Packet (1981) argued that a star fed by an accretion disk reaches Keplerian rotation after accreting just a few percent of its initial mass. It remains unclear whether a star rotating at this speed can continue to accrete mass. In the models by Petrovic et al. (2005) and de Mink et al. (2009b), it was assumed that accretion ceases when the star reaches the Keplerian limit. Only in short-period systems can tides spin down the accreting star such that it can undoubtedly resume accreting a substantial amount of mass. Popham & Narayan (1991) argue that viscous coupling between the star and the disk can govern an inward flow of mass and an outward flow of angular momentum such that mass gainers in wider binaries may also continue to accrete while rotating near or at the Keplerian limit. While we are not in a position to resolve this debate, we have the tools to investigate the impact of both extreme assumptions on the distribution of rotation rates. In our standard simulation we follow Popham & Narayan (1991). Following Petrovic et al. (2005) instead does not reduce the number of stars that are spun up, but it does reduce the mass and therefore brightness of these stars. As a result we find that the fraction of rapid rotators in our brightness limited sample changes by -11%.

5.2.3. Mixing and Mass Loss during Mergers?

Mergers constitute the least understood phase of binary evolution. In particular, the amount of mass loss and the amount of mixing are uncertain. In our standard simulations we assume that a fraction $\mu_{\rm loss} = 0.1$ of the total system mass is lost during a merger and that a fraction $\mu_{\rm mix} = 0.1$ of the envelope is mixed into the core. Changing the amount of mass lost affects the number of mergers that are bright enough to be included in the sample, but the effect is small. Varying $\mu_{\rm loss}$ in the range 0–0.25 results in a change that is not larger than $\pm 0.4\%$. Changing the amount of mixing primarily changes the remaining lifetime of the merger product. Varying $\mu_{\rm mix}$ in the range 0–1 to simulate the effect of no additional mixing versus complete mixing of the core and the envelope, we find a change of -0.8% and $+2.5\%$, respectively.

5.2.4. Magnetic Fields?

Recent searches have revealed large-scale magnetic fields in several O-type stars (e.g., Wade et al. 2012c) with strengths large enough to affect their spin-down time (Ud-Doula et al. 2009). Several recent findings may be relevant for our study. The apparent single O-star HD 148937 was shown to host a large-scale magnetic field (Hubrig et al. 2008, 2011; Nazé et al. 2010; Wade et al. 2012a), and is a strong candidate for being a merger product (Langer 2012). It is surrounded by a bipolar nebula that

may have been ejected during the merger event. Furthermore, the recent detection of a large-scale magnetic field in the mass gainer of Plaskett's star (Grunhut et al. 2013) implies that such fields can exist in a star shortly after an accretion event, and may even indicate that such fields can be generated as its result. In this context it is interesting to mention the tentative detection of a magnetic field in the O-star of Cyg-X1 by Karitskaya et al. (2010; see, however, Bagnulo et al. 2012), and for HD 153919 (Hubrig et al. 2011), which is the O-star companion to the $\sim$2.5 $M_{\odot}$ compact object 4U1700-37 (cf. Clark et al. 2002).

If the production of a large-scale magnetic field would be a common by-product of a mass transfer or merger event (e.g., Ferrario et al. 2009; Tutukov & Fedorova 2010) or if it could be generated as a result of a rotationally driven dynamo (e.g., Potter et al. 2012a), we would have underestimated the spin-down times of such products (e.g., Meynet et al. 2011). Since this scenario is speculative at the moment, we refrain from quantifying such an effect, but it might reduce the number of rapidly rotating stars produced by binary interaction. It would not, however, decrease the number of binary products in a given population (S. E. de Mink et al. 2013, in preparation).

6. DISCUSSION AND IMPLICATIONS

Based on our simulations we expect 20^{+5}_{-10}% of massive main-sequence stars to rotate rapidly as a result of binary interaction. In this section, we discuss implications for rotationally induced mixing in stars (Section 6.1), and for our understanding of the origin of Be stars (Section 6.2). We place our results in the context of the observed distribution of rotation rates (Section 6.3), and we discuss how to proceed from here to derive the true birth spin distribution of massive stars (Section 6.4).

6.1. Implications for Rotationally Induced Mixing

Rotation has been argued to be a major factor influencing the evolution of massive stars. In particular, it is thought to induce mixing in the radiative layers of massive stars (Maeder & Meynet 2000b; Heger et al. 2000, and references therein). The presence of hydrogen-burning products at the surface of O- and B-type stars has generally been interpreted as a signature of rotational mixing (Gies & Lambert 1992; Hunter et al. 2008a; Przybilla et al. 2010). Hunter et al. (2008a) analyzed about a hundred early B-type main-sequence stars in the LMC with projected rotational velocities of up to $\sim$300 km s^{-1}. The rapid rotators with enhanced nitrogen abundances in this sample have been considered to provide the most direct evidence for rotational mixing (Maeder et al. 2009; Brott et al. 2011a).

Our results question the validity of this interpretation; they suggest that a significant fraction, or perhaps even close to all, of the rapid rotators are the products of close binary evolution (see Acke et al. 2008 for a potential exception). Detailed models show that mass transfer in a binary results in surface nitrogen enrichment that covers the observed range (Wellstein et al. 2001; Langer 2012). If the observed nitrogen enrichment of the rapid rotators is primarily the result of mass transfer, there must be less room for rotational mixing (Langer et al. 2008; Brott et al. 2011b).

Additional evidence for the importance of close binary evolution in the sample of Hunter et al. (2008a) comes from the star-by-star analysis of Köhler et al. (2012). They conclude that 10 of the rapidly rotating stars in the sample cannot be explained by rotating single stellar models; the observed nitrogen abundance for these stars is much lower than expected for their age and their projected rotation rate. To reconcile these objects with the theory of rotational mixing requires the assumption that these stars were slow rotators for most of their lives, and that they have been spun up only recently due to close binary interaction by non-conservative mass transfer. We conclude that it is (so far) difficult to single out the effect of rotational mixing in samples of massive main-sequence stars. It turns out that the strategy to circumvent this problem by removing identified binaries from the observed sample is not effective; it may even achieve the opposite. As argued in de Mink et al. (2011), the products of binary evolution typically are or appear to be single stars. As most of the stars which are found to be a member of a binary system did not yet gain any mass from their companion, removing stars with evidence for binarity from the sample may in fact increase the relative contamination of the sample with post-interaction binary products (S. E. de Mink et al. 2013, in preparation).

We conclude that the role of rotational mixing remains ambiguous at present. This is unsatisfying given the large implications of rotational mixing on the evolution of the progenitors of long gamma-ray bursts and pair-instability supernovae (e.g., Yoon et al. 2006; Woosley & Heger 2006; Langer et al. 2007) as well as on the chemical and radiative feedback of massive stars, in particular in the early universe (e.g., Ekström et al. 2008a; Yoon et al. 2012). Further studies of the relation between rotation rates and nitrogen surface abundances of large and well-defined samples of stars are essential. A first step may be to establish whether the types of behavior seen in B-stars are also present in O-stars.

6.2. Evidence for Spin-up from Be/X-Ray Binaries and the Binary Origin of Be Stars

Compelling evidence for spin-up of massive main-sequence stars as a result of binary interaction comes from the Be/X-ray binaries, the most common type of high-mass X-ray binaries (Liu et al. 2006). This class, first recognized by Maraschi et al. (1976), consists of a neutron star in an eccentric orbit around a rapidly rotating B-main-sequence star. The formation of these systems can be understood by assuming that the progenitor of the neutron star transferred mass and angular momentum to its companion before it exploded as a supernova (Rappaport & van den Heuvel 1982). The Be/X-ray binaries constitute the subset of systems that remained bound after the explosion. The majority of the systems is, however, expected to be disrupted as a result of the kick of the neutron star, thereby producing single Be stars (e.g., Blaauw 1961; Eldridge et al. 2011).

The idea that a significant fraction, or even all, of the Be stars result from binary interaction has been explored by Pols et al. (1991) and van Bever & Vanbeveren (1997). Both studies conclude that binaries provide a significant fraction of single Be stars, but they also find that the number of mass transfer systems is not high enough to explain all Be stars. However, our models show that binaries produce significantly more rapid rotators than given in these studies. This is partially due to the fact that we consider stellar mergers as a channel to form rapid rotators. Furthermore, the initial binary parameter distributions adopted in these original studies were based on Abt (1983) and Abt & Levy (1978). We adopt distributions based on recent work (Sana et al. 2012b), which made clear that earlier studies underestimated the frequency of short-period binaries for O-stars (Sana et al. 2012b).

We refrain from predicting the fraction of Be stars produced by our models because the precise conditions for the

Table 2
A Compilation of Observational Studies Listing the Percentages of Stars, F, with Projected Rotational Velocities Larger than 200, 300, and 400 km s^{-1}

Reference	Environment	Sp. Type	Sample Size	$F_{>200\,\mathrm{km\,s^{-1}}}$ (%)	$F_{>300\,\mathrm{km\,s^{-1}}}$ (%)	$F_{>400\,\mathrm{km\,s^{-1}}}$ (%)
Observed samples						
Conti & Ebbets (1977)	MW	O	205	26	10	0
Howarth et al. (1997)	MW	OB	373	9	4	1
Abt et al. (2002)	MW	B0-3	357	16	4	0.3
Martayan et al. (2006)	LMC (NGC 2004)	B	121	15	7	0
Martayan et al. (2007)	SMC (NGC 330)	B	198	27	9	1.0
Hunter et al. (2008b)	LMC	OB	204	16	2	0
" "	SMC	OB	204	22	6	0
Penny & Gies (2009)	MW	OB	97	22	10	1
" "	LMC	OB	106	8	9	0
" "	SMC	OB	55	13	5	0.2
Huang et al. (2010)	MW (Clusters)	B0-9	695	28	7	0.1
" "	MW (Field)	B0-9	483	19	5	0
VLT-FLAMES Tarantula Survey (VFTS)						
Dufton et al. (2013)	LMC (30 Dor)	O9.5-B3	337	50	15	3
O. Ramírez-Agudelo et al. (2013, in preparation)	LMC (30 Dor)	O	178	30	16	5
Predictions from this work						
" "	All			19	11	2
" "	Mergers			5	3	0.5
" "	Other			14	8	1.5

Be phenomenon remain somewhat elusive. It is, however, worth mentioning that the total fraction of mergers and mass gainers in our standard simulation is 24.1% (cf. the top right panel of Figure 4). For comparison, the fraction of Be stars among early-type, non-supergiant B-type stars is 20%–30% after correcting for selection effects (Zorec & Briot 1997).

6.3. Comparison with Observed Samples

A direct comparison between the various observational results, summarized in Table 2, and our predictions is difficult due to different selection and methodological effects and potentially different age distributions of the respective stellar populations. For example, some observational studies attempt to identify and remove spectroscopic binaries while others did not. Furthermore, some samples are biased against rapid rotators, for example, because emission line stars were not included or because of an inherited bias in samples that are based on archival spectra. A comparison with our predictions should thus also be taken with care. Overall, however, we find remarkable trends which appear to be present in all samples.

The fraction of stars with $v \sin i > 200\,\mathrm{km\,s^{-1}}$ in the observed samples compiled in Table 2 ranges between 10% and 50%, while our calculations predict numbers of the order of 20%, all produced from binaries. Our theoretical number is based on the assumption of a constant star formation rate. We expect that for certain star formation histories, e.g., a starburst, and certain observational biases, e.g., in samples focusing on the cluster turnoff, the rates may be significantly different over the situation captured by our models (e.g., Pols & Marinus 1994; van Bever & Vanbeveren 1998; Chen & Han 2008, F. R. N. Schneider et al. 2013, in preparation).

Considering higher cutoff values for $v \sin i$ appears to leave less and less room for single stars, even considering the error margin in our prediction (cf. Section 5). Above 300 km s^{-1}, only the Dufton et al. (2013) and O. Ramírez-Agudelo et al. (2013, in preparation) samples, both resulting from the VLT-FLAMES Tarantula Survey (VFTS), find more stars than we predict. The latter works however have removed detected spectroscopic binaries from their sample, which account for almost a third of their total sample. As can be seen from Figure 4, spectroscopic binaries are expected to mostly contribute to the $v \sin i$ distribution below 300 km s^{-1}. If we correct our predictions for this we obtain $F_{>300\,\mathrm{km\,s^{-1}}} = 16\%$, which is remarkably close to what is observed in the VFTS samples.

This trend continues when considering stars above 400 km s^{-1}. While the number of observed stars is small, the associated percentages from the VFTS samples are close to our results. We note that the VFTS samples do not suffer from an explicit bias against the most rapid rotators, in contrast to the other samples. Whether this is sufficient to explain the observational differences with the VFTS results or whether there is a genuine difference between the rotational properties of stars in 30 Dor and stars in less extreme environments would require a careful assessment of the selection effects and observational biases of these other samples.

The above analysis suggests a decreasing fraction of genuine single stars in stellar samples with increasing $v \sin i$ cutoff. It appears possible that there is a $v \sin i$ threshold above which binary products dominate the population. To establish such a threshold, and its error bar, requires tailored binary population models which reproduce specific observed samples; this is beyond the scope of this paper. Nevertheless, from the preliminary comparison of our models with the existing data in Table 2 it seems conceivable that this threshold value—which will depend on metallicity, star formation history, and sample biases—could generally be smaller than 300 km s^{-1}.

6.4. Toward Deriving the Initial Distribution of Rotation Rates

Deriving the initial distribution of rotation rates is a high priority given its importance as a constraint for star formation theories (e.g., Rosen et al. 2012) and as input condition for modeling populations of massive stars both nearby and at high redshift (Brott et al. 2011b; Levesque et al. 2012; Eldridge & Stanway 2009). In the literature, it is often assumed that the distribution of rotation rates of early-type stars closely reflects their birth spin distribution, arguing that the rotational velocity

of massive stars is not expected to change significantly during their main-sequence evolution—which we do confirm when considering only genuine single stars. However, we have shown that this assumption does not generally hold, due to the large close binary fraction of massive stars (Sana et al. 2012b) and the consequences of close binary evolution.

For star clusters or a star formation rate which is strongly peaked in time, the effects may be smaller (e.g., for extremely young star clusters) or larger (looking at the main-sequence turnoff of star clusters, where all stars are close to ending core hydrogen burning). Since star clusters that are much younger than the lifetime of their most massive stars are difficult to find, it may remain a challenge to derive the true birth distribution of the spins of massive stars directly from observations.

There may be two promising ways to proceed. One may try to observe the birth spin distribution of massive stars directly in young star clusters, excluding the most massive stars. If such kinds of studies are successful, the $v \sin i$ distribution can be compared with those of stars in the same mass range, for older clusters, where binary effects had time to operate. This could be compared with results from our method, with tailored input functions appropriate for the observed samples, which would allow us to draw conclusions about the effects of binary evolution. Alternatively, our method may be used in the future to directly derive the initial spin distribution of an observed population, adopting an iterative process where this distribution is varied until the observations are appropriately reproduced.

S.d.M. acknowledges the Argelander Institute of Bonn University for hospitality during various visits. We thank the members of the VLT-FLAMES massive stars consortium (PI: C. Evans) and especially Ines Brott, Philip Dufton, Paul Dunstall, John Eldridge, Evert Glebbeek, Eveline Helder, Danny Lennon, Colin Norman, Stan Owocki, Oscar Ramírez-Agudelo, Fabian Schneider, and Nolan Walborn for fruitful discussion or commenting on early versions of this paper. In particular, we are indebted to Onno Pols for comments and his contributions and updates made over the years to the original Fortran version of the code. Furthermore we thank the referee for suggestions to enhance the clarity of the discussion.

Support for this work was provided by NASA through Hubble Fellowship grant HST-HF-51270.01-A awarded by the Space Telescope Science Institute, which is operated by the Association of Universities for Research in Astronomy, Inc., for NASA, under contract NAS 5- 26555. We also acknowledge partial support by the National Science Foundation under grant No. 1066293 and the hospitality of the Aspen Center for Physics.

APPENDIX

RAPID BINARY EVOLUTIONARY CODE

In Section 2 we briefly described the rapid binary evolutionary code employed in this study. Here, we provide a more complete description with references and document routines that have not been documented elsewhere.

A.1. Stellar Wind Mass Loss

To account for the radiatively driven winds of massive stars we implement the mass-loss prescription of Vink et al. (2000, 2001). This recipe accounts for the fast increase of the mass-loss rate for stars with temperatures below 22,000 K, which is related to the recombination of Fe IV to Fe III and is commonly referred to as the bi-stability jump. Following Brott et al. (2011a), we perform a linear interpolation in the mass-loss rate within 2500 K of the jump, to ensure a continuous transition.

To accommodate the strong mass-loss increase when approaching the Humphreys & Davidson (1994) limit, we switch to the empirical mass-loss rate of Nieuwenhuijzen & de Jager (1990) at any temperature lower than the critical temperature for the bi-stability jump, when the Vink et al. (2001) rate becomes smaller than that from Nieuwenhuijzen & de Jager (1990). This ensures a smooth transition between the two mass-loss prescriptions and naturally accounts for the increased mass loss at the theoretically predicted second bi-stability jump at ∼12,500 K.

We adopt Wolf–Rayet mass-loss rates of Hamann et al. (1995) for naked helium stars and stars with thin hydrogen envelopes (Hurley et al. 2000). To account for the extreme mass loss of stars beyond the Humphreys–Davidson limit a luminous blue variable like mass-loss rate is included as described in Hurley et al. (2000). Mass-loss rates during the evolved stages of intermediate- and low-mass stars are based on Kudritzki & Reimers (1978) and Vassiliadis & Wood (1993); see Hurley et al. (2000).

The prescription by Vink et al. (2001) accounts for the metallicity dependence of radiatively driven winds with a scaling factor of $(Z/0.02)^{0.85}$, where Z is the metallicity expressed as the initial mass fraction of elements heavier then helium. We apply the same scaling to the Nieuwenhuijzen & de Jager (1990) rates. Other rates are assumed not to depend significantly on metallicity (e.g., van Loon 2006).

A.2. Effects of Rotation

Throughout the evolution of each binary system we compute how the stellar spins change as a result of their internal evolution and angular momentum loss and gain by tides, mass exchange, and stellar winds.

A.2.1. Internal Evolution and the Moment of Inertia

As the star evolves, its moment of inertia, $I = kMR^2$, where k is the radius of gyration squared, changes. The original implementation described in Hurley et al. (2000) assumed a constant $k = 0.1$ during the main sequence. However, even over the course of the main sequence the evolution of the internal structure significantly changes (e.g., Ekström et al. 2008b). Therefore, we adopt fitting formula (O. R. Pols 2010, private communication) for the evolution and mass dependence of the gyration radius based on evolutionary models by Pols et al. (1998). For zero-age main-sequence stars, the gyration radius squared, k_0, is given by

$$k_0 \simeq c + \min\{0.21, \max\{0.09 - 0.27 \log M, \times 0.037 + 0.033 \log M\}\}, \quad \text{(A1)}$$

where the correction factor $c = 0$, except for stars with $\log M > 1.3$, for which $c = -0.055(\log M - 1.3)^2$. When the stars evolve along the main sequence, the star becomes more centrally condensed and the gyration radius decreases. This can be described in terms of the radius R and the radius at zero-age R_0,

$$k \simeq (k_0 - 0.025)\left(\frac{R}{R_0}\right)^C + 0.025\left(\frac{R}{R_0}\right)^{-0.1}, \quad \text{(A2)}$$

where

$$C = \begin{cases} -2.5 & \log M < 0, \\ -2.5 + 5 \log M & \text{for } 0 < \log M < 0.2, \\ -1.5 & 0.2 < \log M. \end{cases} \quad \text{(A3)}$$

Although our fits are based on models at a metallicity $Z = 0.02$, we account for the main effect of metallicity through the dependence of the radii on metallicity, as a result of the choice to express k in terms of R/R_0. This approximation is sufficient for our purposes. Analytic approximations of the evolution of the gyration radius at more evolved evolutionary stages are included as well, but the differences with respect to the original implementation by Hurley et al. (2000) do not significantly affect our study.

We assume that the internal rotational profile can be approximated by the assumption of rigid rotation as a result of efficient internal transport of angular momentum. For main-sequence stars, this is supported by the findings of detailed stellar models (Ekström et al. 2008b; Brott et al. 2011a), independent of the detailed treatment of the internal angular momentum transport processes.

A.2.2. Deformation by Rotation and the Keplerian Limit

Stars become oblate when they rotate near their Keplerian limit, i.e., the rotation rate for which material at the equator is no longer bound to the star because the outward centrifugal acceleration balances the inward gravitational acceleration. Deviations from spherical symmetry have been observed directly by interferometric studies, for example, by Altair and Alchernar (Peterson et al. 2006; Carciofi et al. 2008). We account for the deformation of rotation as described in Section 2. To obtain the equatorial radii we compute the shape of the equipotential surface in the Roche approximation. Under the assumption that the polar radius is not affected by rotation this becomes an algebraic equation of the third degree (e.g., Maeder 2009). We find that the numerical solution obtained by the Newton method can be approximated by the following analytic approximation

$$\log_{10} \frac{R_{\rm eq}}{R_{\rm p}}(\omega) \simeq \omega \, (f_1 \tan[1.422\,\omega] + f_2 \sin[\omega]), \qquad \text{(A4)}$$

where $f_1 = 1.7539 \times 10^{-2}$ and $f_2 = 4.511 \times 10^{-2}$, which can be evaluated in the timely fashion required for population synthesis. We note that there is also some ambiguity in the literature with respect to these two possible definitions of "the fraction of breakup" expressed in terms of the rotation rate, Ω and in terms of the rotational velocity $v_{\rm eq}$. Note that $\Omega/\Omega_{\rm K} \neq v_{\rm eq}/v_{\rm eq,K}$ (e.g., Maeder 2009). For slow and intermediate rotation rates, the fraction of breakup in terms of the rotation rate and the fraction of breakup in terms of the rotational velocity deviate by a factor 0.67 since

$$\frac{v_{\rm eq}}{v_{\rm eq,K}} = \frac{R_{\rm eq}}{R_{\rm eq,K}} \Omega/\Omega_{\rm K}. \qquad \text{(A5)}$$

A.2.3. The Interplay of Rotation and the Stellar Wind

To account for the effect of rotation on the mass loss by stellar winds we follow the approach by Maeder & Meynet (2000a, Equation (4.30)). They derive the latitudinal mass flux from a star deformed by rotation taking into account the effect of gravity darkening (von Zeipel 1924),

$$\frac{\dot{M}(\omega)}{\dot{M}(0)} \simeq \left(\frac{1-\Gamma}{1-\Gamma-f(\omega)} \right)^{\frac{1}{\alpha}-1}, \qquad \text{(A6)}$$

where Γ is the Eddington factor and α is the force multiplier, for which we use the empirical relation by Lamers et al. (1995) valid for $\log T_{\rm eff} = 3.9$–4.7, where α varies from 0.15 to 0.52. Outside this range, we assume that α is independent of the effective temperature. The dependence on the rotation rates enters through

$$f(\omega) = \frac{\Omega}{2\pi G \rho_m} \approx 0.198 \left(\omega \frac{R_{\rm eq}}{R_{\rm p}}(\omega) \right)^2. \qquad \text{(A7)}$$

The approximation on the right-hand side is accurate up to $\omega \lesssim 0.8$. We compute the Eddington factor,

$$\Gamma = \frac{\kappa L}{4\pi c G M}, \qquad \text{(A8)}$$

by approximating the opacity κ with the electron scattering opacity, $\kappa \simeq 0.2(1 + X)$, where X is the mass fraction of hydrogen at the surface. Since we do not explicitly follow the surface composition we adopt $X = 0.74$ for stars that still have a hydrogen envelope and $X = 0$ for naked helium stars.

In this prescription the effect of rotation on the mass-loss rate is small (Maeder & Meynet 2000a). Only for $\Gamma > 0.64$ and $\log T_{\rm eff} \leqslant 4.3$ is a large increase of the mass-loss rate predicted. In all cases we limit the stellar wind mass-loss rate to the thermal mass-loss rate $\dot{M}_{\rm KH} \equiv M/\tau_{\rm KH}$, where we approximate the Kelvin–Helmholtz timescale $\tau_{\rm KH}$ as

$$\tau_{\rm KH} = 10^7 \, {\rm yr} \frac{M}{RL}, \qquad \text{(A9)}$$

where M, R, and L refer to the current mass, radius, and luminosity expressed in solar units, respectively.

The radiatively driven stellar wind of a star deformed by rotation becomes aspherical as a result of the changes of the effective gravity with latitude. Georgy et al. (2011) computed the net effect of the latitudinal dependence on the loss of angular momentum. They find that the deviation from the spherical cases is very small. In the interest of computational speed we can therefore safely assume that the specific angular momentum of mass lost through the stellar wind is equal to $j = 2/3 R_p^2 \Omega$.

A.2.4. Mass and Angular Momentum Loss of Stars Rotating Close to Keplerian Rotation

During their lifetime, stars may approach the Keplerian rotation rate as a result of mass accretion (Packet 1981) or as a result of internal evolution (Ekström et al. 2008b). In this case, the star must dispose of its excess angular momentum at a rate dictated by the process that drives the star to its Keplerian limit. If angular momentum loss by stellar wind or tides is not efficient enough, it is likely that a near-Keplerian disk is formed when the thermal motion of gas particles at the equator becomes sufficient to overcome the escape speed, such that they are launched into orbit around the star (Okazaki & Negueruela 2001). Viscous coupling of the disk and the star may help extract angular momentum efficiently (Paczynski 1991; Sills et al. 2005; Krtička et al. 2011) while losing only very little mass, depending on the viscosity and the extent of the disk. The disk may be truncated by the torque of the companion star. A further possibility is the illumination of the disk which may cause it to flare and disperse. The interplay between these processes will determine how much mass the rapidly rotating star can accrete. A detailed treatment of outflowing disks within a binary system is beyond the purpose of this study, but we discuss the effects of extreme assumptions in Section 5.2.

A.3. Treatment of Binary Interaction

A.3.1. Mass Transfer Rate

We model mass transfer as described in Hurley et al. (2002), but with the following adaptations. In the original version of the code the rate for stable mass transfer is assumed to be a steep function of the amount by which the star overfills its Roche lobe (Hurley et al. 2002, Equation (58)). This prescription can introduce numerical instabilities, causing the star to oscillate in and out of its Roche lobe. Therefore, we replace this prescription by an adaptive algorithm. When the star fills its Roche lobe we determine the mass transfer rate by removing a small amount of mass and computing the resulting change in radius until the stellar radius becomes smaller than the Roche lobe radius within a certain threshold. The rate is capped by the thermal rate as defined in Hurley et al. (2002, Equation (60)). As a result, the mass transfer rate is governed by the evolutionary changes in the stellar radius and changes in the Roche lobe.

When a star accretes mass on timescales that are short compared to the thermal timescale the accreting star may be driven out of thermal equilibrium resulting in expansion (Benson 1970). The severity of this effect is uncertain as it depends on the poorly constrained specific entropy of the accreted material. Shocks during the accretion process may result in the accretion of lower entropy material (Shu & Lubow 1981). Most detailed binary evolutionary codes use simple boundary conditions where material is assumed to be accreted with the specific entropy of the surface of the accretor. This leads to severe expansion in binaries with extreme mass ratios, implying that a large fraction of the systems will come in contact with the likely result of a stellar merger. Due to the practical limitations of the design of our rapid code, we cannot follow the radii of stars during the accretion process. To account for systems that come in contact as a result of this effect, we adopt a critical mass ratio for main-sequence binaries, $q_{\rm crit,MS}$, and assume that the stars come in contact when $M_{\rm acc}/M_{\rm don} < q_{\rm crit,MS}$, where $M_{\rm don}$ is the mass of the Roche lobe-filling star and $M_{\rm acc}$ is the mass of the companion. This critical mass ratio depends only weakly on the separation (de Mink et al. 2007). We therefore consider two free parameters $q_{\rm crit,MS}$ and $q_{\rm crit,HG}$ which set the critical mass ratio for systems that interact on the main sequence and systems in which the donor star fills its Roche lobe while it is crossing the Hertzsprung gap. Our standard value $q_{\rm crit,MS} = 0.65$ is based on detailed binary evolutionary models (de Mink et al. 2007) and for $q_{\rm crit,HG}$ we adopt a value of 0.4. For the advanced evolutionary stages we follow Hurley et al. (2002).

A.3.2. Rejuvenation and the Convective Core

If the accreting star is a main-sequence star we assume that it adapts its interior structure to its new mass. This implies that the convective core grows, such that fresh hydrogen is mixed into the central regions, effectively rejuvenating the accreting star. We treat this by adapting the effective fractional main-sequence lifetime as in Tout et al. (1997). The original implementation implicitly assumed that the size of the convective core is a fixed fraction of 10% of the stellar mass. This strongly underestimates the core mass for massive main-sequence stars found in detailed models and ignores the fact that the mass fraction of the convective core increases with stellar mass. To improve this we adopt the fit formula provided by Glebbeek & Pols (2008) for the effective core mass at the end of the main sequence as a function of the initial stellar mass. We do not account for the shrinkage of the convective core over the course of the main-sequence evolution.

A.3.3. Transfer of Angular Momentum Accretion

When mass is transferred through the interior Lagrange point to the secondary star it may either form an accretion disk around the secondary star or it may directly impact on the surface of the secondary star. Direct evidence for this is found in the Hα profiles in Algol-type binaries (Richards & Albright 1999).

To distinguish between direct impact and the formation of an accretion disk we estimate the minimum $R_{\rm min}$ distance between the stream and the accreting star using an analytic fit by Ulrich & Burger (1976) against calculations of Lubow & Shu (1975) to determine whether the stream will hit the star (O. R. Pols 2010, private communication). Lubow & Shu (1975) estimate the specific angular momentum of the impact stream to be equal to $\sqrt{GM1.7R_{\rm min}}$. If the impact parameter is larger than the radius of the accretor, then the stream is assumed to collide with itself after which the viscous process leads to the formation of a Keplerian accretion disk. The star is assumed to accrete from the inner radius of the disk, where gas particles accrete with the specific angular momentum of a Keplerian orbit with a radius equal to the stellar radius $\sqrt{GMR_{\rm eq}}$.

Packet (1981) pointed out that, under these assumptions, the accreting star is very efficiently driven toward the Keplerian limit after accreting only a few percent of its own mass in the case of accretion via a disk. In our standard models set, we will follow the argument of Paczynski (1991) and Popham & Narayan (1991) who argue that a star rotating at the Keplerian limit can keep accreting mass from an accretion disk without accreting angular momentum as a result of viscous coupling.

While the star rotates near the Keplerian limit the net accreted angular momentum is slowly reduced below the specific angular momentum of a Keplerian orbit as discussed by Colpi et al. (1991). There is some debate whether an equilibrium situation may be reached at a sub-Keplerian rotational velocity, for example, in the presence of a magnetic field (Ghosh & Lamb 1979; Pringle 1989). If this equilibrium is reached at a very small fraction of the Keplerian rate it would affect the results in this study, similar to that discussed in Section 5.2.4.

A.3.4. Wind Accretion

We consider wind accretion (Bondi & Hoyle 1944) with adopting an efficiency factor $\alpha_{\rm BH} = 1.5$ as detailed in Hurley et al. (2002). However, in contrast to Hurley et al. we assume that the specific angular momentum from material gained by wind accretion is small and can be ignored (cf. Ruffert 1999).

A.3.5. Treatment of Stellar Mergers

A large fraction of massive stars are found in binaries that are expected to evolve into contact systems and eventually merge (Benson 1970; Wellstein et al. 2001). The mergers that are of main interest for this study are those that result from the merger of two main-sequence stars. We use the extensive grid of detailed binary evolutionary models (de Mink et al. 2007) to calibrate the critical mass ratio for close binaries leading to contact systems.

For the treatment of mergers involving an evolved star, we follow Hurley et al. (2002). The original prescription for mergers involving two main-sequence stars assumes that the merger product is completely mixed and that no mass is lost during the process. These assumptions in combination with the original prescription that severely underestimated the mass of

the convective core for massive main-sequence stars implied that the mergers experience severe rejuvenation placing them near the zero-age main sequence.

We adapt the treatment of mergers between two main-sequence stars with respect to the original implementation to better reflect current insights and detailed models. We assume that a certain fraction $\mu_{\rm loss}$ of the combined mass is lost from the system when two stars merge. In our standard simulation we adopt a fraction of 10% in our standard simulations in agreement with Lombardi et al. (1995, 1996). Note, however, that these simulations are for direct collisions, not for merging binaries. We therefore consider $\mu_{\rm loss}$ one of the uncertain parameters. We assume that the mass lost from the system originates from the stellar envelopes and is not enriched in helium. We assume that after a short phase lasting a thermal timescale the merger product will settle and can be described as a star rotating near the Keplerian rate.

Whether merger products experience significant mixing is uncertain (e.g., Gaburov et al. 2008). To mimic the result of smoothed particle hydrodynamic simulations, which show remarkably little mixing occurring when two stars merge, we envision in our standard model that the core of the most evolved star settles in the center of the merger surrounded by the core of its companion. The most evolved star is not necessarily the primary star. We then assume that the merger product develops a convective core of a mass that can be approximated by the prescriptions given by Glebbeek & Pols (2008). Depending on how much mass is lost from the system, the new convective core mass may be larger or smaller than the combined mass of both original cores.

We consider the possibility that an additional amount of mass just above the convective core can be mixed into the central regions. To this extent we introduce a second parameter $\mu_{\rm mix}$ which expresses the mass of this region as a fraction of the envelope mass. We adopt $\mu_{\rm mix} = 0.1$ as a standard option (Gaburov et al. 2008). Setting $\mu_{\rm mix} = 1$ allows for complete mixing of the merger product after mass loss. We work out the new relative age by considering which regions are mixed and following the approach by Hurley et al. (2002) to use a simple linear map between the core composition and the relative age.

In this new approach, which uses a more realistic approximation for the core size, the mergers are the relative age of the merger product is only slightly smaller than the relative age of the original primary star. In other words, we now provide a more conservative estimate of the remaining lifetime of the merger products.

A.3.6. Common Envelope Evolution

To treat common envelope situations we follow Hurley et al. (2002) we use choose a common envelope ejection efficiency parameter $\alpha_{\rm CE} = 0.2$ in agreement with studies of binary systems in planetary nebulae (Zorotovic et al. 2010; Davis et al. 2010; De Marco et al. 2011). For the parameter describing the binding energy of the envelope $\lambda_{\rm CE}$ we use fits to Dewi & Tauris (2000) and we adopt $\lambda_{\rm ionization} = 0.5$. We note that in the original version of the code massive stars are not treated as convective giants when they become red supergiants after the ignition of helium. We corrected this using the base of the giant branch as a transition point. During common envelope evolution we assume that the companion does not accrete mass nor angular momentum. Our results are not sensitive to these assumptions.

REFERENCES

Abt, H. A. 1983, ARA&A, 21, 343
Abt, H. A., Levato, H., & Grosso, M. 2002, ApJ, 573, 359
Abt, H. A., & Levy, S. G. 1978, ApJS, 36, 241
Acke, B., Verhoelst, T., van den Ancker, M. E., et al. 2008, A&A, 485, 209
Bagnulo, S., Landstreet, J. D., Fossati, L., & Kochukhov, O. 2012, A&A, 538, A129
Benson, R. S. 1970, PhD thesis, Univ. California, Berkeley
Blaauw, A. 1961, BAN, 15, 265
Bodenheimer, P. 1995, ARA&A, 33, 199
Bondi, H., & Hoyle, F. 1944, MNRAS, 104, 273
Brott, I., de Mink, S. E., Cantiello, M., et al. 2011a, A&A, 530, A115
Brott, I., Evans, C. J., Hunter, I., et al. 2011b, A&A, 530, A116
Carciofi, A. C., Domiciano de Souza, A., Magalhães, A. M., Bjorkman, J. E., & Vakili, F. 2008, ApJL, 676, L41
Chen, X., & Han, Z. 2008, MNRAS, 384, 1263
Claeys, J. S. W., de Mink, S. E., Pols, O. R., Eldridge, J. J., & Baes, M. 2011, A&A, 528, A131
Clark, J. S., Goodwin, S. P., Crowther, P. A., et al. 2002, A&A, 392, 909
Colpi, M., Nannurelli, M., & Calvani, M. 1991, MNRAS, 253, 55
Conti, P. S., & Ebbets, D. 1977, ApJ, 213, 438
Daflon, S., Cunha, K., de Araújo, F. X., Wolff, S., & Przybilla, N. 2007, AJ, 134, 1570
Davis, P. J., Kolb, U., & Willems, B. 2010, MNRAS, 403, 179
De Becker, M., Rauw, G., Manfroid, J., & Eenens, P. 2006, A&A, 456, 1121
De Marco, O., Passy, J.-C., Moe, M., et al. 2011, MNRAS, 411, 2277
de Mink, S. E., Cantiello, M., Langer, N., et al. 2009a, A&A, 497, 243
de Mink, S. E., Langer, N., & Izzard, R. G. 2011, BSRSL, 80, 543
de Mink, S. E., Pols, O. R., & Hilditch, R. W. 2007, A&A, 467, 1181
de Mink, S. E., Pols, O. R., Langer, N., & Izzard, R. G. 2009b, A&A, 507, L1
Dervişoğlu, A., Tout, C. A., & Ibanoğlu, C. 2010, MNRAS, 406, 1071
Dewi, J. D. M., & Tauris, T. M. 2000, A&A, 360, 1043
Donati, J.-F., & Landstreet, J. D. 2009, ARA&A, 47, 333
Dufton, P. L., Langer, N., Dunstall, P. R., et al. 2013, A&A, in press (arXiv:1212.2424)
Ekström, S., Georgy, C., Eggenberger, P., et al. 2012, A&A, 537, A146
Ekström, S., Meynet, G., Chiappini, C., Hirschi, R., & Maeder, A. 2008a, A&A, 489, 685
Ekström, S., Meynet, G., Maeder, A., & Barblan, F. 2008b, A&A, 478, 467
Eldridge, J. J., Langer, N., & Tout, C. A. 2011, MNRAS, 414, 3501
Eldridge, J. J., & Stanway, E. R. 2009, MNRAS, 400, 1019
Ferrario, L., Pringle, J. E., Tout, C. A., & Wickramasinghe, D. T. 2009, MNRAS, 400, L71
Friend, D. B., & Abbott, D. C. 1986, ApJ, 311, 701
Gaburov, E., Lombardi, J. C., & Portegies Zwart, S. 2008, MNRAS, 383, L5
Georgy, C., Meynet, G., & Maeder, A. 2011, A&A, 527, A52
Georgy, C., Meynet, G., Walder, R., Folini, D., & Maeder, A. 2009, A&A, 502, 611
Ghosh, P., & Lamb, F. K. 1979, ApJ, 234, 296
Gies, D. R., & Lambert, D. L. 1992, ApJ, 387, 673
Glebbeek, E., Gaburov, E., de Mink, S. E., Pols, O. R., & Portegies Zwart, S. F. 2009, A&A, 497, 255
Glebbeek, E., & Pols, O. R. 2008, A&A, 488, 1017
Grunhut, J. H., Wade, G. A.., Leutenegger, M., et al. 2013, MNRAS, 428, 1686
Hamann, W.-R., Koesterke, L., & Wessolowski, U. 1995, A&A, 299, 151
Hartmann, L., & Stauffer, J. R. 1989, AJ, 97, 873
Heger, A., & Langer, N. 2000, ApJ, 544, 1016
Heger, A., Langer, N., & Woosley, S. E. 2000, ApJ, 528, 368
Hilditch, R. W., Howarth, I. D., & Harries, T. J. 2005, MNRAS, 357, 304
Hillwig, T. C., Gies, D. R., Bagnuolo, W. G., Jr., et al. 2006, ApJ, 639, 1069
Hirschi, R., Meynet, G., & Maeder, A. 2004, A&A, 425, 649
Howarth, I. D., Siebert, K. W., Hussain, G. A. J., & Prinja, R. K. 1997, MNRAS, 284, 265
Huang, W., Gies, D. R., & McSwain, M. V. 2010, ApJ, 722, 605
Hubrig, S., Schöller, M., Kharchenko, N. V., et al. 2011, A&A, 528, A151
Hubrig, S., Schöller, M., Schnerr, R. S., et al. 2008, A&A, 490, 793
Humphreys, R. M., & Davidson, K. 1994, PASP, 106, 1025
Hunter, I., Brott, I., Lennon, D. J., et al. 2008a, ApJL, 676, L29
Hunter, I., Lennon, D. J., Dufton, P. L., et al. 2008b, A&A, 479, 541
Hurley, J. R., Pols, O. R., & Tout, C. A. 2000, MNRAS, 315, 543
Hurley, J. R., Tout, C. A., & Pols, O. R. 2002, MNRAS, 329, 897
Hut, P. 1981, A&A, 99, 126
Izzard, R. G., Dray, L. M., Karakas, A. I., Lugaro, M., & Tout, C. A. 2006, A&A, 460, 565
Izzard, R. G., Glebbeek, E., Stancliffe, R. J., & Pols, O. R. 2009, A&A, 508, 1359

Izzard, R. G., Tout, C. A., Karakas, A. I., & Pols, O. R. 2004, MNRAS, 350, 407
Karitskaya, E. A., Bochkarev, N. G., Hubrig, S., et al. 2010, IBVS, 5950, 1
Kippenhahn, R., & Weigert, A. 1967, ZA, 65, 251
Köhler, K., Borzyszkowski, M., Brott, I., Langer, N., & de Koter, A. 2012, A&A, 544, A76
Kroupa, P. 2001, MNRAS, 322, 231
Krtička, J., Owocki, S. P., & Meynet, G. 2011, A&A, 527, A84
Krumholz, M. R. 2011, ApJ, 743, 110
Krumholz, M. R., Klein, R. I., McKee, C. F., Offner, S. S. R., & Cunningham, A. J. 2009, Sci, 323, 754
Kudritzki, R.-P., & Puls, J. 2000, ARA&A, 38, 613
Kudritzki, R. P., & Reimers, D. 1978, A&A, 70, 227
Lamers, H. J. G. L. M., Snow, T. P., & Lindholm, D. M. 1995, ApJ, 455, 269
Langer, N. 1998, A&A, 329, 551
Langer, N. 2012, ARA&A, 50, 107
Langer, N., Cantiello, M., Yoon, S.-C., et al. 2008, in IAU Symp. 250, Massive Stars as Cosmic Engines, ed. F. Bresolin, P. A. Crowther, & J. Puls (Cambridge: Cambridge Univ. Press), 167
Langer, N., Norman, C. A., de Koter, A., et al. 2007, A&A, 475, L19
Larson, R. B. 2010, RPPh, 73, 014901
Lauterborn, D. 1970, A&A, 7, 150
Levesque, E. M., Leitherer, C., Ekstrom, S., Meynet, G., & Schaerer, D. 2012, ApJ, 751, 67
Liu, Q. Z., van Paradijs, J., & van den Heuvel, E. P. J. 2006, A&A, 455, 1165
Lombardi, J. C., Jr., Rasio, F. A., & Shapiro, S. L. 1995, ApJL, 445, L117
Lombardi, J. C., Jr., Rasio, F. A., & Shapiro, S. L. 1996, ApJ, 468, 797
Lubow, S. H., & Shu, F. H. 1975, ApJ, 198, 383
Maeder, A. 2009, Physics, Formation and Evolution of Rotating Stars (Berlin: Springer)
Maeder, A., & Meynet, G. 2000a, A&A, 361, 159
Maeder, A., & Meynet, G. 2000b, ARA&A, 38, 143
Maeder, A., Meynet, G., Ekström, S., & Georgy, C. 2009, CoAst, 158, 72
Maraschi, L., Treves, A., & van den Heuvel, E. P. J. 1976, Natur, 259, 292
Martayan, C., Frémat, Y., Hubert, A.-M., et al. 2006, A&A, 452, 273
Martayan, C., Frémat, Y., Hubert, A.-M., et al. 2007, A&A, 462, 683
Mason, B. D., Gies, D. R., Hartkopf, W. I., et al. 1998, AJ, 115, 821
Mason, B. D., Hartkopf, W. I., Gies, D. R., Henry, T. J., & Helsel, J. W. 2009, AJ, 137, 3358
McKee, C. F., & Ostriker, E. C. 2007, ARA&A, 45, 565
Mestel, L. 1965, QJRAS, 6, 161
Meynet, G., Eggenberger, P., & Maeder, A. 2011, A&A, 525, L11
Mokiem, M. R., de Koter, A., Evans, C. J., et al. 2006, A&A, 456, 1131
Mokiem, M. R., de Koter, A., Vink, J. S., et al. 2007, A&A, 473, 603
Nazé, Y., Ud-Doula, A., Spano, M., et al. 2010, A&A, 520, A59
Neo, S., Miyaji, S., Nomoto, K., & Sugimoto, D. 1977, PASJ, 29, 249
Nieuwenhuijzen, H., & de Jager, C. 1990, A&A, 231, 134
Okazaki, A. T., & Negueruela, I. 2001, A&A, 377, 161
Packet, W. 1981, A&A, 102, 17
Paczynski, B. 1991, ApJ, 370, 597
Penny, L. R., & Gies, D. R. 2009, ApJ, 700, 844
Peterson, D. M., Hummel, C. A., Pauls, T. A., et al. 2006, ApJ, 636, 1087
Petrovic, J., Langer, N., & van der Hucht, K. A. 2005, A&A, 435, 1013
Podsiadlowski, P., Joss, P. C., & Hsu, J. J. L. 1992, ApJ, 391, 246
Pols, O. R. 1994, A&A, 290, 119
Pols, O. R., Cote, J., Waters, L. B. F. M., & Heise, J. 1991, A&A, 241, 419
Pols, O. R., & Marinus, M. 1994, A&A, 288, 475
Pols, O. R., Schröder, K.-P., Hurley, J. R., Tout, C. A., & Eggleton, P. P. 1998, MNRAS, 298, 525
Pols, O. R., Tout, C. A., Schröder, K.-P., Eggleton, P. P., & Manners, J. 1997, MNRAS, 289, 869
Popham, R., & Narayan, R. 1991, ApJ, 370, 604
Potter, A. T., Chitre, S. M., & Tout, C. A. 2012a, MNRAS, 424, 2358
Potter, A. T., Tout, C. A., & Eldridge, J. J. 2012b, MNRAS, 419, 748
Pringle, J. E. 1989, MNRAS, 236, 107
Przybilla, N., Firnstein, M., Nieva, M. F., Meynet, G., & Maeder, A. 2010, A&A, 517, A38
Rappaport, S., & van den Heuvel, E. P. J. 1982, in IAU Symp. 98, Be Stars, ed. M. Jaschek & H.-G. Groth (Cambridge: Cambridge Univ. Press), 327
Rauw, G., Nazé, Y., Fernández Lajús, E., et al. 2009, MNRAS, 398, 1582
Richards, M. T., & Albright, G. E. 1999, ApJS, 123, 537
Rosen, A. L., Krumholz, M. R., & Ramirez-Ruiz, E. 2012, ApJ, 748, 97
Ruffert, M. 1999, A&A, 346, 861
Salpeter, E. E. 1955, ApJ, 121, 161
Sana, H., de Koter, A., de Mink, S. E., et al. 2012a, A&A, in press (arXiv:1209.4638)
Sana, H., de Mink, S. E., de Koter, A., et al. 2012b, Sci, 337, 444
Sana, H., & Evans, C. J. 2011, in IAU Symp. 272, Active OB Stars: Structure, Evolution, Mass Loss, and Critical Limits, ed. C. Neiner, G. Wade, G. Meynet, & G. Peters (Cambridge: Cambridge Univ. Press), 474
Sana, H., Gosset, E., & Evans, C. J. 2009, MNRAS, 400, 1479
Sana, H., Gosset, E., Nazé, Y., Rauw, G., & Linder, N. 2008, MNRAS, 386, 447
Sana, H., James, G., & Gosset, E. 2011, MNRAS, 416, 817
Schröder, K.-P., Pols, O. R., & Eggleton, P. P. 1997, MNRAS, 285, 696
Shu, F. H., & Lubow, S. H. 1981, ARA&A, 19, 277
Sills, A., Adams, T., & Davies, M. B. 2005, MNRAS, 358, 716
Skumanich, A. 1972, ApJ, 171, 565
Soderblom, D. R., Stauffer, J. R., MacGregor, K. B., & Jones, B. F. 1993, ApJ, 409, 624
Tout, C. A., Aarseth, S. J., Pols, O. R., & Eggleton, P. P. 1997, MNRAS, 291, 732
Townsend, R. H. D., Owocki, S. P., & Howarth, I. D. 2004, MNRAS, 350, 189
Tutukov, A. V., & Fedorova, A. V. 2010, ARep, 54, 156
Tylenda, R., Hajduk, M., Kamiński, T., et al. 2011, A&A, 528, A114
Ud-Doula, A., Owocki, S. P., & Townsend, R. H. D. 2009, MNRAS, 392, 1022
Ulrich, R. K., & Burger, H. L. 1976, ApJ, 206, 509
van Bever, J., & Vanbeveren, D. 1997, A&A, 322, 116
van Bever, J., & Vanbeveren, D. 1998, A&A, 334, 21
van Loon, J. T. 2006, in ASP Conf. Ser. 353, Stellar Evolution at Low Metallicity: Mass Loss, Explosions, Cosmology, ed. H. J. G. L. M. Lamers, N. Langer, T. Nugis, & K. Annuk (San Francisco, CA: ASP), 211
Vassiliadis, E., & Wood, P. R. 1993, ApJ, 413, 641
Vink, J. S., de Koter, A., & Lamers, H. J. G. L. M. 2000, A&A, 362, 295
Vink, J. S., de Koter, A., & Lamers, H. J. G. L. M. 2001, A&A, 369, 574
von Zeipel, H. 1924, MNRAS, 84, 665
Wade, G. A., Grunhut, J., Gräfener, G., et al. 2012a, MNRAS, 419, 2459
Wade, G. A., Grunhut, J. H., & the MiMeS Collaboration. 2012b, in ASP Conf. Proc. 464, Circumstellar Dynamics at High Resolution, ed. A. Carciofi & Th. Rivinius (San Francisco, CA: ASP), 405
Wade, G. A., Maíz Apellániz, J., Martins, F., et al. 2012c, MNRAS, 425, 1278
Wellstein, S., Langer, N., & Braun, H. 2001, A&A, 369, 939
Wolff, S. C., Strom, S. E., Cunha, K., et al. 2008, AJ, 136, 1049
Woods, T. E., & Ivanova, N. 2011, ApJL, 739, L48
Woosley, S. E., & Heger, A. 2006, ApJ, 637, 914
Yoon, S.-C., Dierks, A., & Langer, N. 2012, A&A, 542, A113
Yoon, S.-C., & Langer, N. 2005, A&A, 443, 643
Yoon, S.-C., Langer, N., & Norman, C. 2006, A&A, 460, 199
Yorke, H. W. 1986, ARA&A, 24, 49
Zahn, J.-P. 1975, A&A, 41, 329
Zahn, J.-P. 1977, A&A, 57, 383
Zorec, J., & Briot, D. 1997, A&A, 318, 443
Zorotovic, M., Schreiber, M. R., Gänsicke, B. T., & Nebot Gómez-Morán, A. 2010, A&A, 520, A86